REPORT DOCUMENTATION PAGE

Form Approved
OMB No. 0704-0188

1. AGENCY USE ONLY (Leave blank)	2. REPORT DATE	3. REPORT TYPE AND DATES COVERED
	Sept 94	Final 2 Jul 92-30 Jun 94

4. TITLE AND SUBTITLE

Diffraction Limited Imaging Using Aberrated Optics

5. FUNDING NUMBERS

DAAL03-92-G-0142

6. AUTHOR(S)

D.A. Fish
E.R. Pike

7. PERFORMING ORGANIZATION NAME(S) AND ADDRESS(ES)

King's College London
The Strand
London WC2R 2LS, U.K.

8. PERFORMING ORGANIZATION REPORT NUMBER

9. SPONSORING/MONITORING AGENCY NAME(S) AND ADDRESS(ES)

U.S. Army Research Office
P.O. Box 12211
Research Triangle Park, NC 27709-2211

10. SPONSORING/MONITORING AGENCY REPORT NUMBER

ARO 30390.1-MA-SDI

11. SUPPLEMENTARY NOTES

The views, opinions and/or findings contained in this report are those of the author(s) and should not be construed as an official Department of the Army position, policy, or decision, unless so designated by other documentation.

12a. DISTRIBUTION/AVAILABILITY STATEMENT

Approved for public release; distribution unlimited.

12b. DISTRIBUTION CODE

13. ABSTRACT *(Maximum 200 words)*

Researchers have introduced a scanning method for SVD reconstruction of images. This method removes the blocking effects that would normally be associated with a reconstruction by parts. It is also vastly superior in terms of computation speed as compared with conventional SVD. The method is also applicable to the case of spatially varying blurs. The results have shown that the blocking effects are removed to a tolerable level with the scanning technique, and good constructions can be obtained with large complex images containing noise. To show the potential for the reconstruction of images formed with a spatially variant PSF and approximate method using Fourier transforms was shown. This introduced artifacts into the reconstruction which were controlled by use of a regularisation parameter. An example reconstruction has been shown for an SVD reconstruction which is more accurate than the Fourier method, but far slower in computational speed.

14. SUBJECT TERMS

Aberrated Optics, Images, Fourier Transforms, Diffraction Limited Imaging

15. NUMBER OF PAGES

43

16. PRICE CODE

17. SECURITY CLASSIFICATION OF REPORT	18. SECURITY CLASSIFICATION OF THIS PAGE	19. SECURITY CLASSIFICATION OF ABSTRACT	20. LIMITATION OF ABSTRACT
UNCLASSIFIED	UNCLASSIFIED	UNCLASSIFIED	UL

Diffraction limited imaging using aberrated optics - Final report

D.A. Fish, E.R. Pike
Physics Department
King's College London
The Strand
London WC2R 2LS, U.K.

9th August 1994

1 Introduction

In this project a requirement for diffraction limited imaging using aberrated optics for space imaging have been considered. The use of large telescopes or arrays of small telescopes in space are subject to time varying aberrations introduced, for example as a result of gravitational fluctuations. To obtain diffraction limited images from aberrated images requires some form of data processing algorithm to reconstruct the original object.

In the past the problem of imaging astronomical objects through a turbulent atmosphere has been achieved using iterative algorithms on large numbers of short exposure, low light level data sets, to reconstruct objects from speckle type images [1] [2]. In contrast the space to space imaging problem requires algorithms capable of reconstructing objects from one or a limited number of data sets in the high level light regime. The proposed research was to tackle this problem in three areas.

1. Blind deconvolution.
2. Image reconstruction using a known aberration function.
3. Exponential filter speckle imaging.

The work performed upon this project has concentrated mainly upon the first two of the above areas. Blind deconvolution involves the retrieval of both object and point spread function (PSF) from a noisy image. This is achieved using iterative algorithms that use *a priori* information about either the object, the PSF or both. Over the duration of the project existing blind deconvolution algorithms have been implemented and new ones developed, and their relative merits accessed. Image reconstruction using a known aberration function has concentrated upon singular value analysis for the data inversion. Comparisons with many other popular techniques have been carried out. Testing upon real data has also been carried out with the use of Hubble space telescope images.

2 Blind deconvolution

The intial algorithm implemented was the Ayers Dainty method [3] and a full testing of this algorithm was performed. Along similar lines a Weiner filter blind deconvolution algorithm and a new algorithm which used the popular Richardson and Lucy deconvolution technique [4,5] as its basis were implemented. Comparisons of the performance of these algorithms were made.

2.1 The Ayres Dainty algorithm

The image formed by an optical system can be represented by an integral equation known as a Fredholm integral equation of the first kind.

$$c(x') = \int_{-\infty}^{\infty} g(x', x) f(x) dx \tag{1}$$

where $c(x)$ is the image, $f(x)$ is the object, and $g(x', x)$ is a spatially varying point spread function (PSF). To simplify the problem the PSF is assumed to be constant in the image plane, i.e. isoplanatic. The above equation then becomes,

$$c(x) = \int_{-\infty}^{\infty} f(x') g(x - x') dx' \tag{2}$$

This form of the imaging equation allows the use of Fourier transforms so that in Fourier space :-

$$C(u) = F(u)G(u) \tag{3}$$

where $C(u)$ is the Fourier transform of $c(x)$ and $F(u)$ and $G(u)$ are the Fourier transforms of $f(x)$ and $g(x)$ respectively.

The problem of finding both object and PSF from knowledge of the convolution, which may also contain noise, is a difficult one. *A priori* knowledge of the object and PSF is limited, but non-negativity is an obvious constraint for incoherent imaging problems. Ayers and Dainty developed an algorithm to try to solve this problem which was essentially a generalisation of the Feinup phase retrieval algorithm [6]. The schematic form of the algorithm is shown in figure 1.

2.1.1 The initial estimate of the function $\tilde{f}_0(x)$

The initial estimate of the object $\tilde{f}_0(x)$ is created by the use of a pseudo-random number generator giving positive values between zero and unity constrained to the extent of the convolution.

2.1.2 Image plane constraints

The image plane constraints upon the functions $\tilde{f}_i(x)$ and $\tilde{g}_i(x)$ help determine what form each function takes. *A priori* knowledge is limited, but it is known that each function as it is created from the inverse filter in Fourier space must be non-negative everywhere. Also each function must lie within the region of the convolution. The non-negativity constraint is implemented in the following way :-

$$\tilde{f}_i(x) = \begin{cases} f_i(x), & \text{if } f_i(x) \geq 0 \text{ and } c(x) > 0; \\ 0, & \text{otherwise.} \end{cases} \tag{4}$$

In the Ayers Dainty algorithm the negative values of the function $\tilde{f}_i(x)$ are redistributed as positive one's to maintain energy conservation within the image space. In our algorithm this was found to be unecessary as Fourier plane scaling which is detailed later takes care of this problem.

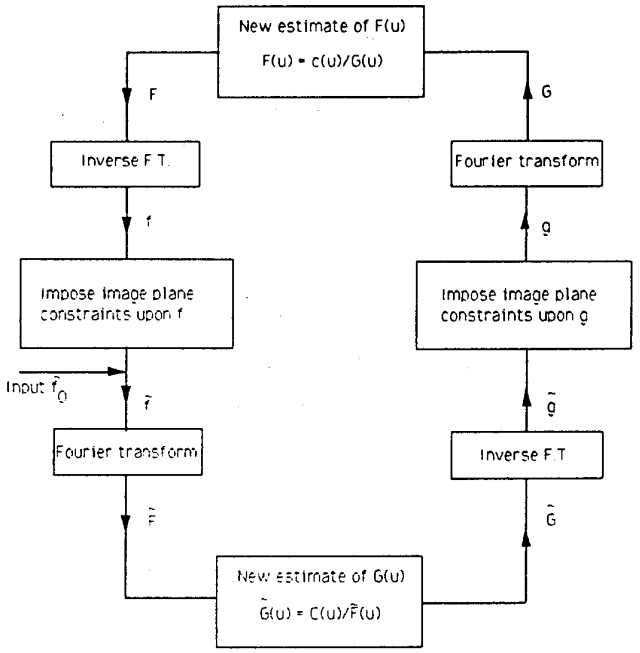

Figure 1. The blind deconvolution algorithm of Ayers and Dainty

2.1.3 Fourier plane constraints

In each iteration the division of two Fourier transforms is required to give the next estimate of the function, i.e.

$$F_{i+1}(u) = \frac{C(u)}{G_i(u)} \tag{5}$$

$$G_{i+1}(u) = \frac{C(u)}{G_i(u)} \tag{6}$$

Instead of performing this operation, an averaging is used which involves incorporating part of the old estimate of the function within the new estimate. Also the division of Fourier transforms can cause problems in areas where either $F_i(u)$ or $G_i(u)$ are small. In this case inverse averaging is performed. These conditions are different from those given in the Ayers Dainty paper. We believe that this paper is in error on this point. The constraints are formalized mathematically as follows :-

If $|C(u)| < \zeta$, where ζ is a noise level in the convolution, then

$$F_{i+1}(u) = \tilde{F}_i(u) \tag{7}$$

If $|C(u)|/|\tilde{G}(u)| \leq \tilde{F}(u)$ then

$$F_{i+1}(u) = (1-\beta)\tilde{F}_i(u) + \beta\frac{|C(u)|}{|\tilde{G}(u)|} \tag{8}$$

If $|C(u)|/|\tilde{G}(u)| \geq \tilde{F}(u)$ then

$$\frac{1}{F_{i+1}(u)} = \frac{(1-\beta)}{\tilde{F}_i(u)} + \beta\frac{|\tilde{G}(u)|}{|C(u)|} \tag{9}$$

where β is the averaging parameter with the constraint $0 \leq \beta \leq 1$. Experience has shown a value of $\beta = 0.7$ appears to give the best results.

2.1.4 Function scaling

It was found that a re-scaling of the functions $f(x)$ and $g(x)$ within the Fourier plane stopped a divergence in intensity of the two functions found when implementing the original Ayres Dainty scheme. This problem could become so bad that one of the functions could 'disappear' below the noise level. The re-scaling was performed before the Fourier plane constraints were applied so that :-

$$S_g = \frac{\sqrt{C(0)}}{\tilde{G}_i(0)} \quad \text{so that} \quad \tilde{G}_i(u) \rightarrow \tilde{G}_i(u)S_g \tag{10}$$

$$S_f = \frac{\sqrt{C(0)}}{\tilde{F}_i(0)} \quad \text{so that} \quad \tilde{F}_i(u) \rightarrow \tilde{F}_i(u)S_g \tag{11}$$

2.1.5 Results of Blind deconvolution using the Ayers Dainty algorithm

Investigation of the effect of noise and object morphology is important for determining how the algorithm will perform under different conditions. It is likely that objects of varying sizes and complexity will appear in real situations, hence performance with respect to object morphology needs to be known. Also real conditions will produce noisy convolutions, therefore the ability of the algorithm to cope with noise has to be determined. Poissonian noise was added to the convolutions by taking the noiseless pixel value as the mean and generating a random number obeying Poissonian statistics to replace this pixel value and hence create the noisy image. A percentage measure to give an indication of the amount of noise upon the image was defined as the standard deviation at the maximum pixel value in the image. This is then the square root of the maximum pixel value divided by that pixel value.

As no stopping criterion exists for the algorithm an error measure, taken as the error between the image and the convolution of the new object and PSF, was formed. The best error object over a specified number of iterations was then taken as the result. Images are shown for the last iteration and the best error iteration.

To test the algorithm in these conditions a simulated satellite was taken as the object, and a speckle type convolution generated with this object. The object and convolution can be seen in figure 2.

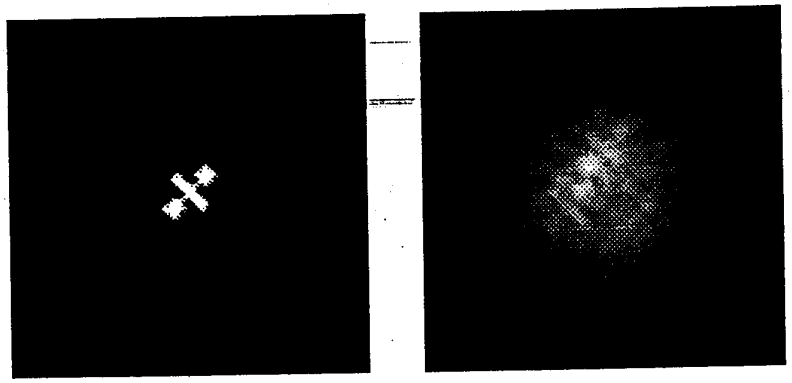

Figure 2. Satellite and convolution

In figure 3a the convolution is noiseless, and both the last iteration and best error objects show a reasonably clear satellite, although they appear under the PSF heading. This is to be expected as the algorithm makes no distinction between the two, also the object and PSF can swap as the algorithm iterates. Up to 150 iterations the errors are very large, but after this point, apart from a few spikes the errors remain comparatively low.

An investigation of the performance of the algorithm in the presence of noise was undertaken. At 0.01% noise in figure 3b the satellite appears remarkably well. In the last iteration results fringes can be seen across the images, especially the PSF, this is characteristic of the change over between object and PSF, and is associated with a large error. This is difficult to see in the error graph, but looking closely reveals a large spike beginning to appear at the last iteration. Further increases in the noise did not produce recognizable objects.

2.1.6 Conclusions

It has been shown here that it is possible to obtain some good reconstructions from the Ayres Dainty algorithm, but as was shown in the first quarterly report the speckle pattern image of the satellite was probably a special case. Also the tolerance to noise was especially poor, therefore other algorithms were considered in light of these drawbacks.

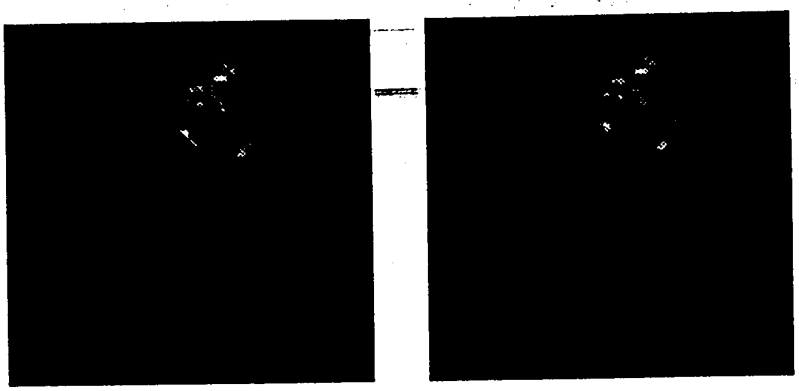

Object, and best error object

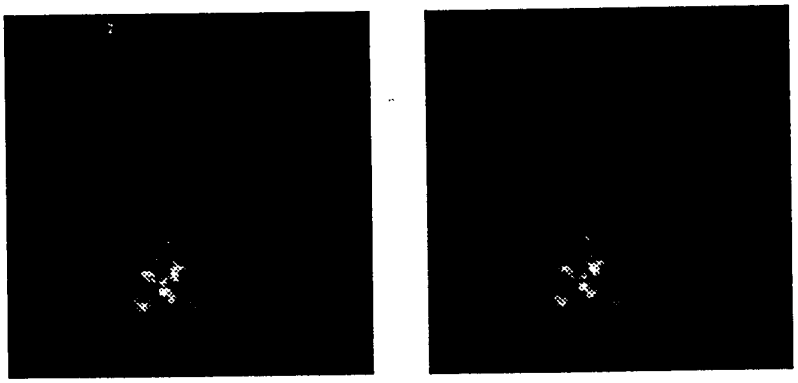

PSF, and best error PSF

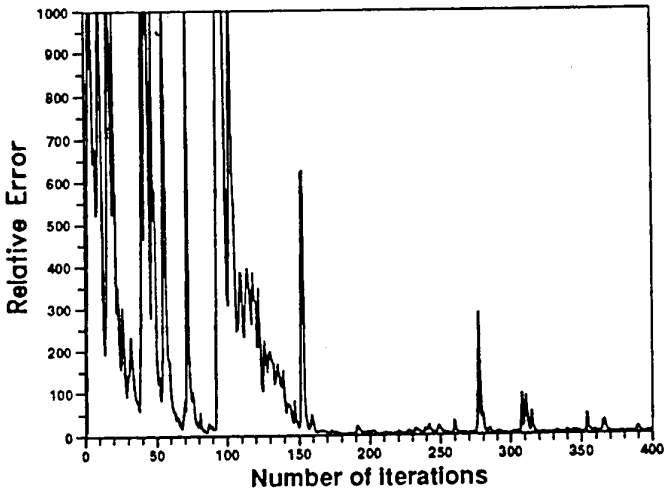

Figure 3a. The blind deconvolution of a satellite from a speckle pattern with zero noise

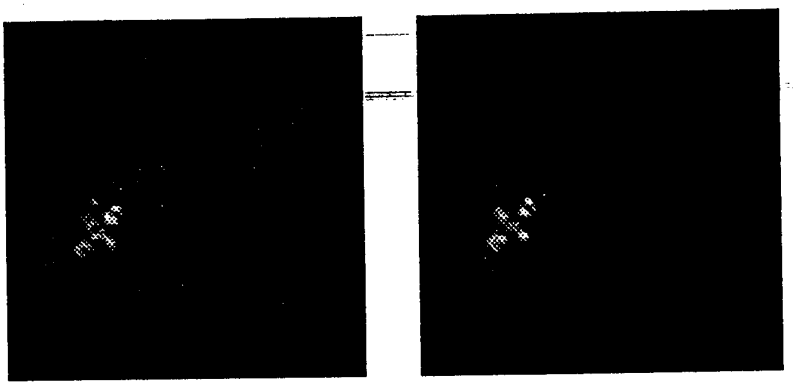

Object, and best error object

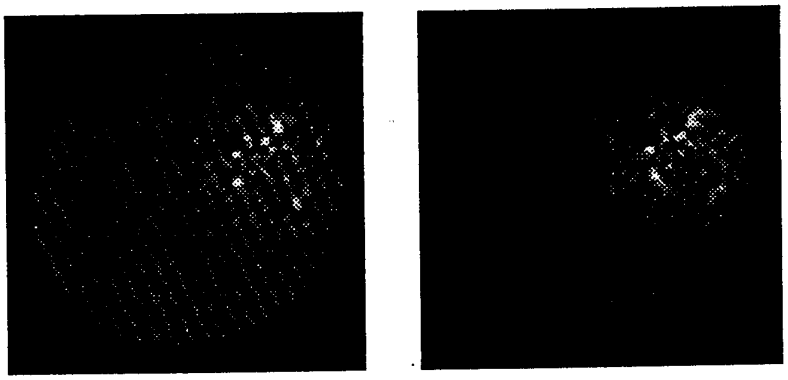

PSF, and best error PSF

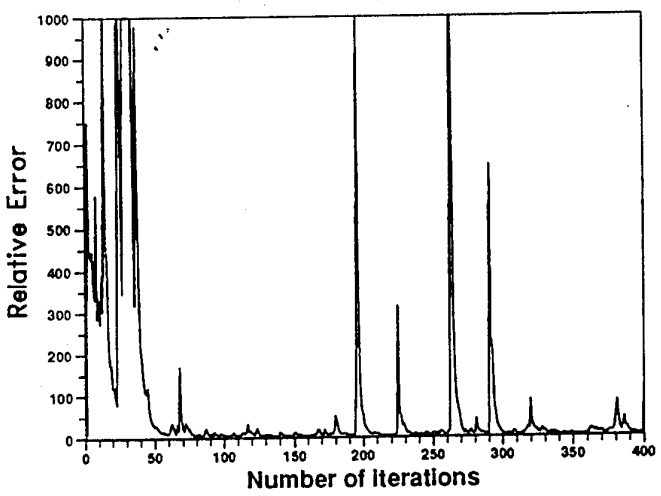

Figure 3b. The blind deconvolution of a satellite from a speckle pattern with 0.01% noise

2.2 Blind deconvolution using a Weiner filter approach

To improve the noise tolerance of the algorithm it was thought that a Weiner filter would be more appropriate than the complicated division in Fourier space method of the Ayres Dainty algorithm. The division in Fourier space is carried out using the modified formula,

$$F(u) = \frac{C(u)\Phi(u)}{G(u)} \tag{12}$$

where $\Phi(u)$ is the optimal or Weiner filter, and is given by,

$$\Phi(u) = \frac{|S(u)|^2}{|S(u)|^2 + |N(u)|^2} \tag{13}$$

with $S(u) = F(u)G(u)$ and where $N(u)$ is the noise spectrum. Hence

$$F(u) = \frac{G^*(u)C(u)}{|G(u)|^2 + \frac{|N(u)|^2}{|F(u)|^2}} \tag{14}$$

The $|N(u)|^2/|F(u)|^2$ term is unknown and is replaced by a constant μ to be determined by experiment.

2.2.1 The Blind Weiner Algorithm

A blind deconvolution algorithm is constructed in the same manner as before but the Fourier plane constraints are replaced by the formula

$$F(u) = \frac{G^*(u)C(u)}{|G(u)|^2 + \mu} \tag{15}$$

when determining $F(u)$, and

$$G(u) = \frac{F^*(u)C(u)}{|F(u)|^2 + \mu} \tag{16}$$

when determining $G(u)$. The image plane constraints and the function scaling in Fourier space remain the same as those used in our form of the Ayres Dainty algorithm. This algorithm is similar to one given by Davey *et al* [7], but there algorithm assumes further *a priori* knowledge in the form of a known object support.

2.2.2 Results

In contrast to the Ayers Dainty algorithm the performance of this algorithm upon speckle type images was particularly poor. It was not possible to obtain any recognizable reconstructions. However, convolutions that used single Gaussians for the PSF faired better. The original object, Gaussian PSF and convolution can be seen in figure 4.

The Ayers Dainty algorithm performed badly upon this type of image, but as can be seen in figure 5a definite cross and Gaussian reconstructions have been found. It was further found that with this type of image and about 1.5% noise, i.e. ≈ 4000 photons in the maximum pixel value of the image, that reconstructions of a similar quality could be obtained, figure 5b.

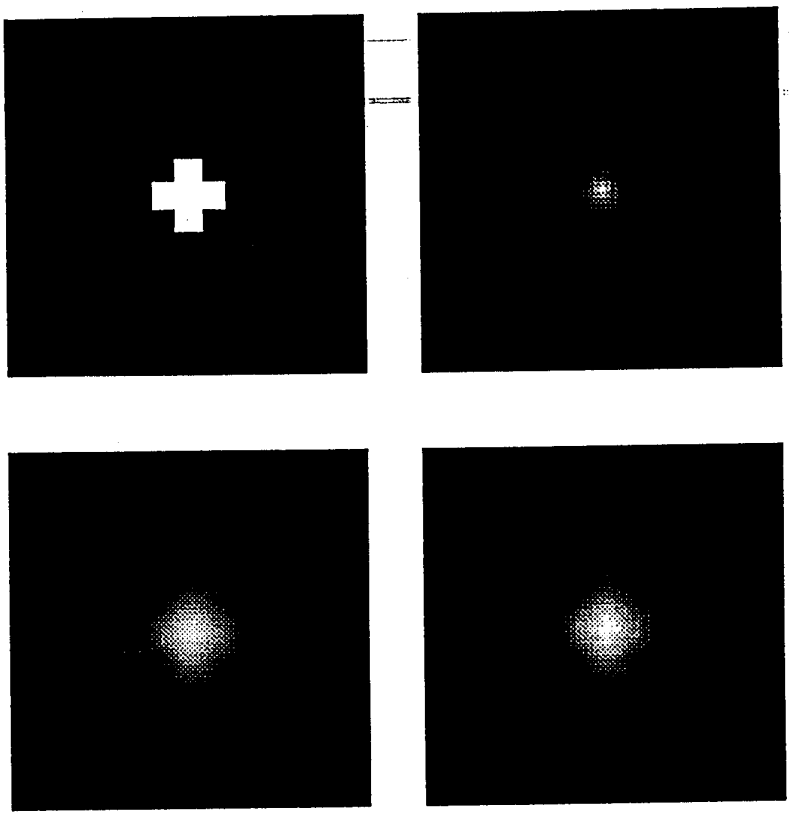

Figure 4. The object, PSF, convolution and convolution with 1.5% noise.

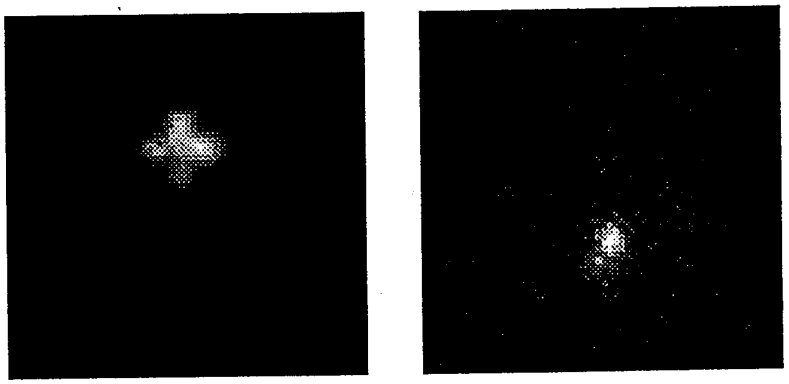

a. Reconstructions with zero noise.

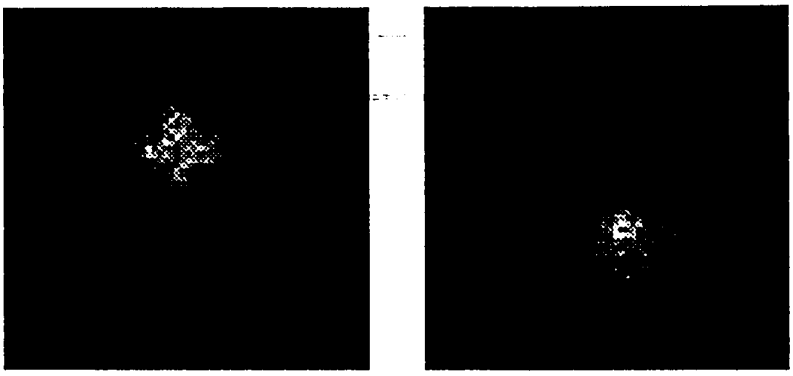

b. Reconstructions with 1.5% noise.

Figure 5. Blind deconvolution using the Weiner filter algorithm.

2.2.3 Conclusions

This section has shown that it is possible to achieve blind deconvolution in the presence of more realistic levels of noise, but for real data it is likely that noise levels will be greater than 1.5% will be encountered. Also the algorithm is still susceptible to the type of image given to it, hence further improvement is still needed.

2.3 Blind deconvolution using the Richardson and Lucy algorithm

The Richardson Lucy deconvolution algorithm has become very popular in the fields of astronomy and medical imaging. Initially it was derived from Bayes theorem in the early seventies by Richardson and Lucy [4,5]. In the early eighties it was rederived by Shepp and Vardi [8] as an algorithm to solve positron emission tomography (PET) imaging problems where Poissonian statistics are dominant. Their method used a maximum likelihood (ML) solution, which was found using the expectation maximization (EM) algorithm of Dempster *et al* [9]. The reason for the popularity of the algorithm is its implementation of ML and its apparent ability to produce reconstructed images of good quality in the presence of high noise levels. We therefore assumed that a blind form of this algorithm would have the same characteristics [10]. A blind deconvolution algorithm similar to the one shown here has also been developed by Holmes [11] using the EM algorithm of Dempster [9].

To begin with a brief review of the Richardson Lucy deconvolution method will be given, then the blind form of the algorithm will be presented. Since Bayes theorem relates conditional probabilities the resulting algorithm takes into account statistical fluctuations in the signal, and therefore has the ability to reconstruct noisy images. Bayes theorem is :-

$$P(x|y) = \frac{P(y|x)P(x)}{\int P(y|x)P(x)dx} \tag{17}$$

where $P(y|x)$ is the conditional probability of an event y given event x. $P(x)$ is the probability of an event x, and $P(x|y)$ is the inverse conditional probability i.e. the probability of event x given event y. The probability $P(x)$ can be identified as the object distribution $f(x)$, the conditional probability $P(y|x)$ can be identified as the PSF centered at x i.e. $g(y,x)$ and the probability $P(y)$ as the degraded image

or convolution $c(y)$. This inverse relation allows the derivation of the iterative algorithm given below.

$$f_{i+1}(x) = \int \frac{g(y,x)c(y)dy}{\int g(y,z)f_i(z)dz} f_i(x) \tag{18}$$

where i is the iteration number. If an isoplanatic condition exists then this equation can be written in terms of convolutions:-

$$f_{i+1}(x) = \left\{ \left[\frac{c(x)}{f_i(x) \otimes g(x)} \right] \otimes g(-x) \right\} f_i(x) \tag{19}$$

where $\otimes$ is the convolution operation. The PSF $g(x)$ is known, so the object $f(x)$ is found by iterating the above equation until convergence. An intial guess is required for the object $f_0(x)$ to start the algorithm. Then in subsequent iterations, due to the form of the algorithm, large deviations in the guess from the true object are lost rapidly in initial iterations whilst detail is added more slowly in subsequent iterations. Advantages of this algorithm include a non-negativity constraint if the initial guess $f_0(x) \geq 0$. Also energy is conserved as the iteration proceeds, which is easily seen by integrating both sides of equation 18 over x.

In the blind form of this algorithm two of these deconvolution steps are required. At the k^{th} blind iteration it is assumed that the object is known from the $k-1$ iteration. The PSF $g^k(x)$ is then calculated for a specified number of Richardson Lucy iterations as in equation 20, where the i index represents the Richardson Lucy iteration. This equation is essentially an inverse of equation 19 since the object and PSF have reverse roles and it calculates the PSF from the object. Then $f^k(x)$ is calculated for the same number of Richardson Lucy iterations. This is done using the PSF evaluated from the full iteration of equation 20. In this case the iteration is performed in the normal manner of equation 19 as shown in equation 21. The degraded image is again given as $c(x)$ in both equations 20 and 21. The loop is repeated as required.

$$g^k_{i+1}(x) = \left\{ \left[\frac{c(x)}{g^k_i(x) \otimes f^{k-1}(x)} \right] \otimes f^{k-1}(-x) \right\} g^k_i(x) \tag{20}$$

$$f^k_{i+1}(x) = \left\{ \left[\frac{c(x)}{f^k_i(x) \otimes g^k(x)} \right] \otimes g^k(-x) \right\} f^k_i(x) \tag{21}$$

The above equations are shown in one dimension, the extension for two dimensional images is straightforward. Starting guesses are made for the object $f^0_0(x)$ and the PSF $g^0_0(x)$ and an algorithm loop of the form of figure 6 is performed. No positivity constraints are required because the above equations always ensure this. The algorithm [10] is different from the Holmes [11] algorithm as only two Richardson Lucy iterations are performed within one blind iteration, one for an object evaluation, and one for the PSF evaluation. It was found that the simulated images used did not perform well with this type of iteration, but when the number of Richardson Lucy iterations with one blind iteration was increased to about ten a much better performance was obtained.

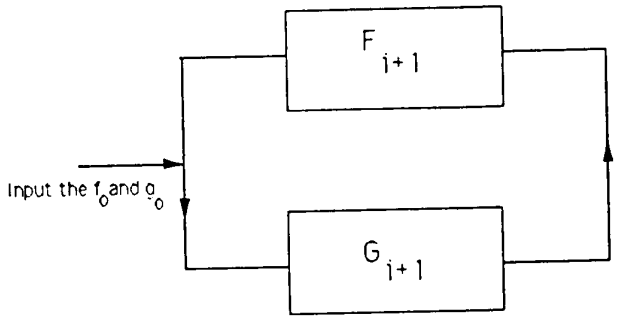

Figure 6. The blind deconvolution algorithm based upon the Richardson and Lucy deconvolution algorithm

2.3.1 Results

In the case of the cross convolved with a Gaussian which gave reasonable results for the Weiner filter algorithm much improved results have been obtained in terms of noise performance. Reconstructions have been obtained when the photon noise was 10%, which allows the possibility of using this algorithm on real data. The convolution can be seen in figure 7a. and the reconstructions of the cross and the Gaussian PSF in figure 7b.

This algorithm was also applied to a speckle image of the cross but failed to produce any recognizable reconstructions. The algorithm was applied to many other images where gaussian PSFs were used and it was found that as long as the blurring of the PSF was not to severe then reasonable reconstructions could generally be obtained, and in some cases with noise levels as high as 15%.

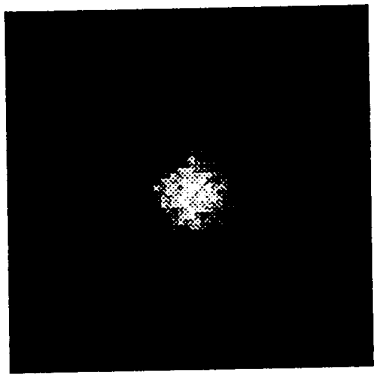

a. The convolution with 10% noise.

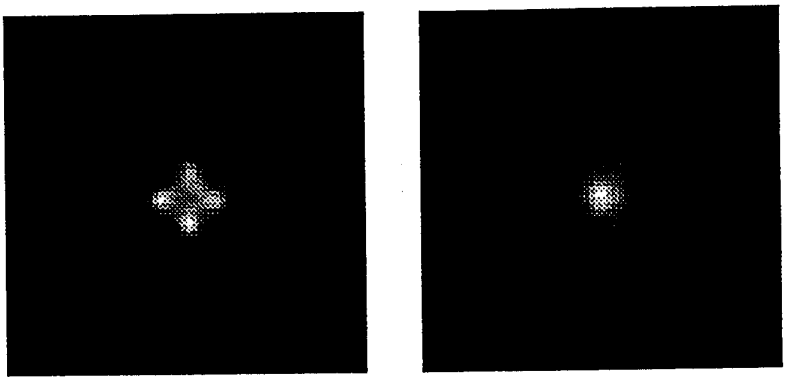

b. Reconstructions of the object and PSF.

Figure 7. Blind deconvolution using the Richardson Lucy algorithm.

2.3.2 Conclusions

As hoped this algorithm has the ability to produce reconstructions at noise levels that are likely to be encountered in real situations. The quality of the reconstructions is good, but the object still significantly blurred. The way to proceed would be the used of further *a priori* information.

3 Semi - Blind deconvolution

It was thought that further *a priori* information could be incorporated by assuming partial knowledge of the form of the PSF. In a real situation it may be known that a telescope suffers from spherical aberration, but due to time varying factors such as a changing gravitational field the extent of this aberration may not be known. This would reduce the number of unknown variables in the deconvolution from maybe thousands of pixel values, to one or two unknown constants. We termed this approach *Semi-Blind deconvolution* [10].

3.1 The Weiner Semi-blind algorithm

This algorithm used the Blind deconvolution using a Weiner filter as its basis. The only part of the algorithm which was altered was the image plane constraints on the PSF. In the blind algorithm this was just non-negativity within the convolution area, and zero outside it. This was replaced by a least squares fitting procedure. Initially convolutions were created with Gaussians, so Gaussians of varying widths were compared to the function input to the routine. The Gaussian giving the least error in fitting was then chosen as the PSF.

To illustrate how well this algorithm performed, figure 8 shows the reconstructions of the object and PSF at every iteration.

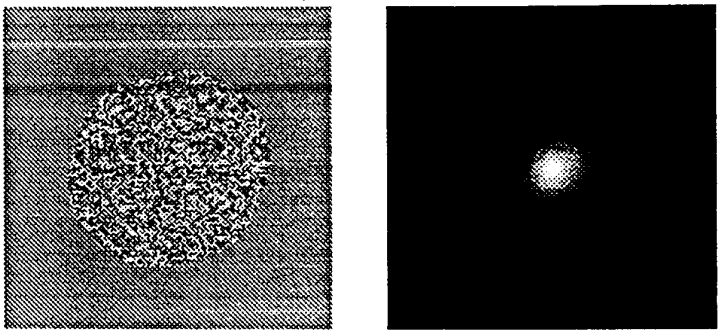

Figure 8a The random guess start for the object, and the convolution

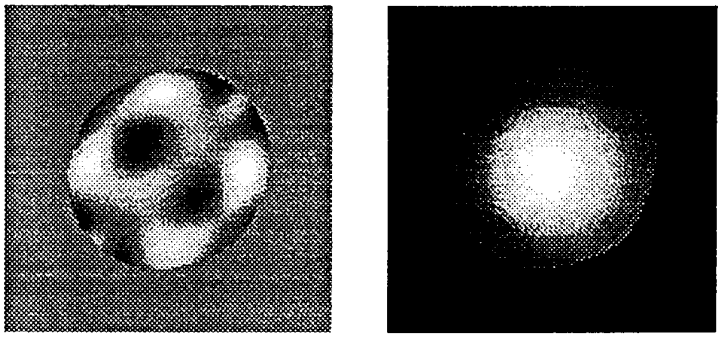

Figure 8b The results from the first iteration

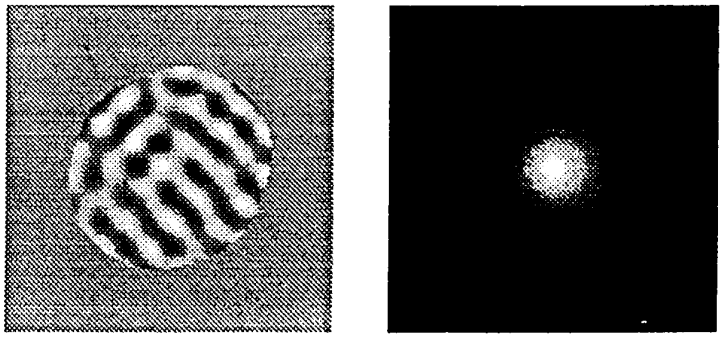

Figure 8c The results from the second iteration

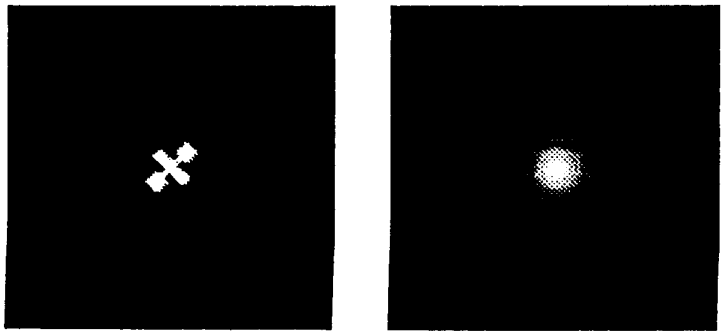

Figure 8d The results from the third iteration

This algorithm has converged within three iterations and has produced a perfect reconstruction of the satellite. The initial convolution was in fact noiseless. When trying to reconstruct with noisy images the algorithm always converged upon the delta function solution i.e. the Gaussian of smallest possible width. Therefore the impressive result obtained in figure 8 would never be found when using real data.

3.2 Semi-blind deconvolution using the Richardson and Lucy algorithm

To try and alleviate the noise tolerance problem the Richardson and Lucy algorithm was tried yet again. The semi-blind form of the algorithm took as its basis the blind algorithm, but in this case a number of blind iterations were performed before fitting a Gaussian to the function it had found for the PSF.

The results for this algorithm have shown remarkable noise tolerance. In figure 9 results are shown for semi-blind deconvolution on a series of point sources. The image contained approximately 20.0% noise.

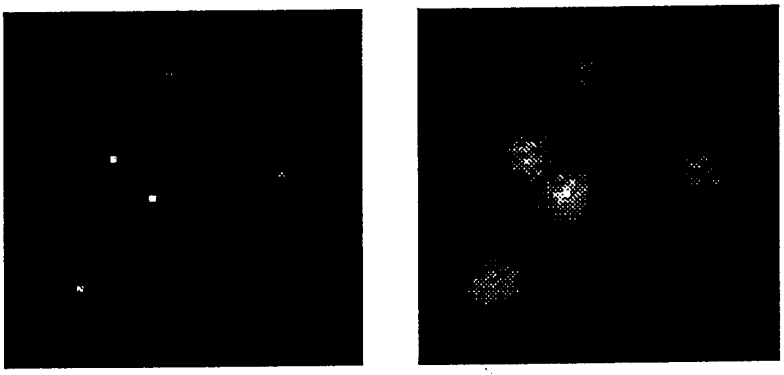

Figure 9a The object and image with 20.0% noise.

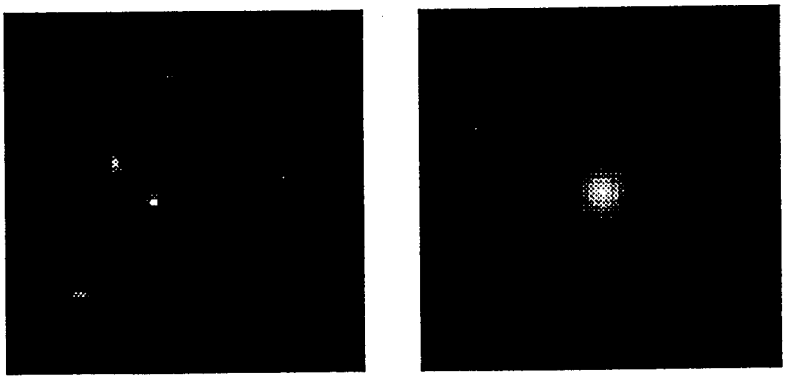

Figure 9b The reconstruction of the object and the chosen fitting Gaussian PSF.

The algorithm was tried on the noisy image of the cross used earlier for the pure blind deconvolution work. Although the PSF was fitted in each iteration with a Gaussian of the correct size the results were not very good, in fact the pure blind deconvolution results were better. Therefore it was decided that a Gaussian fitting process should be performed after the blind deconvolution, and then a specified

number of Richardson-Lucy iteration performed with the guessed Gaussian. The step width in Gaussian fitting was obviously important, with the step width been one pixel for the Gaussian radius at the $1/e$ height the correct PSF width of 3 pixels was guessed. At a step width of 0.1 pixels the Gaussian width obtained was 3.2 pixels. The results for both cases can be seen below.

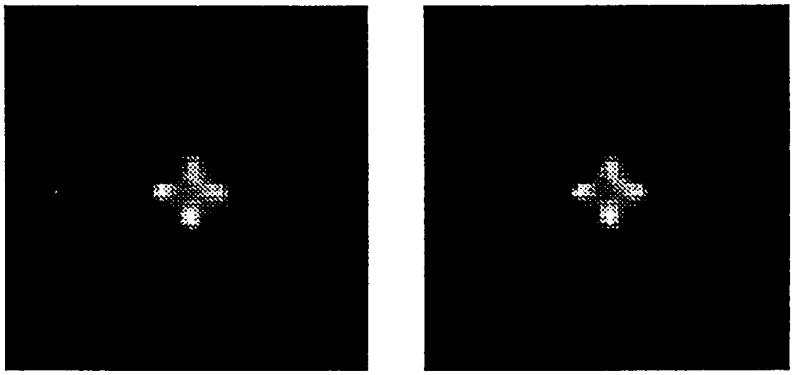

Figure 10 The reconstructions of the cross of figure 4 with Gaussian step widths of 1.0 and 0.1 pixels.

The results show that the slight error made in finding the width of the Gaussian PSF do not make the reconstructions significantly worse. This is probably due to the high level of noise upon the image resulting in a loss of a large amount of information. To show the impressiveness of these results straight forward deconvolutions using Fourier regularisation and the Richardson Lucy are shown in figure 11.

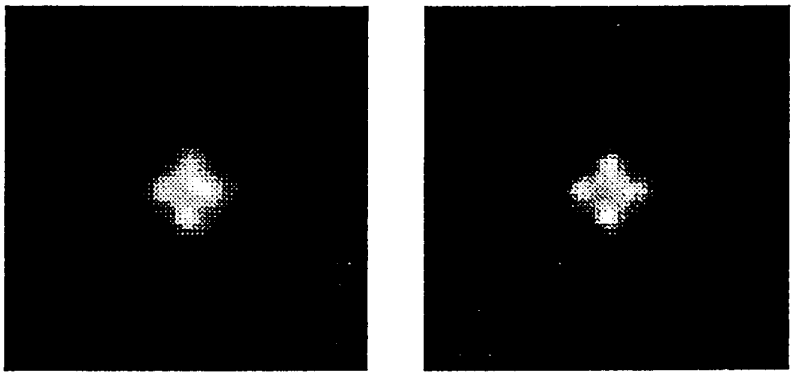

Figure 11 Reconstructions using (a) Fourier regularisation (b) Richardson and Lucy.

It can be seen that the semi-blind deconvolution results are comparable to the usual methods of deconvolution.

To extend this work to use in realistic situations more than one fitting variable may be needed to describe the PSF accurately. To test this a simple PSF was created with the functional form

$$y(r) = \sum_k \left[\frac{A_k \exp(1.0) r^2}{{C_k}^2} + B_k \right] \exp(-\frac{r^2}{{C_k}^2}) \qquad (22)$$

where r is the radius and the variables A_k, B_k, C_k were given the following values:-

$$A_1 = 0.0, \quad A_2 = 0.05$$

$$B_1 = 1.0, \quad B_2 = 0.0$$

$$C_1 = 1.0, \quad C_2 = 5.0$$

The variables A_2, C_1, C_2 were allowed to change their values, so that the PSF was a Gaussian plus a Gaussian times its radius squared. Incorrect values for these variables were entered into the program and a PSF created. Then as before a blind deconvolution process evaluated a new object and PSF. A PSF with the above functional form and free variables A_2, C_1, C_2 was fitted to the evaluated PSF using a Levenberg-Marquardt non-linear, least squares fitting routine. This returned new values for A_2, C_1, C_2, and the process was repeated for a specified number of iterations. The PSF and noiseless convolution can be seen in figure 12, the object was the cross shown earlier.

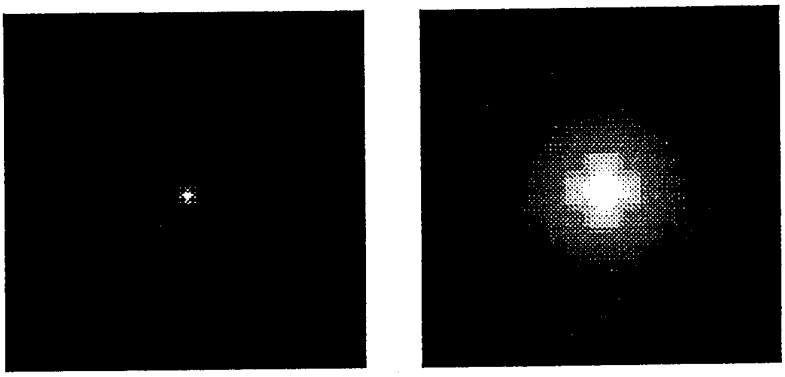

Figure 12 (a) PSF (b) Convolution.

To compare the results of this semi-blind deconvolution algorithm a Richardson and Lucy deconvolution was performed using the known PSF. The result of this can be seen in figure 13.

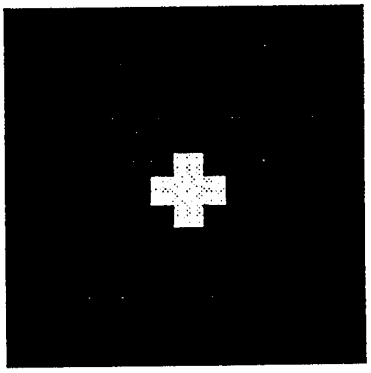

Figure 13 The Richardson Lucy deconvolution of the above image with the above PSF

This can be compared with the results of 15 iterations of the semi blind deconvolution algorithm.

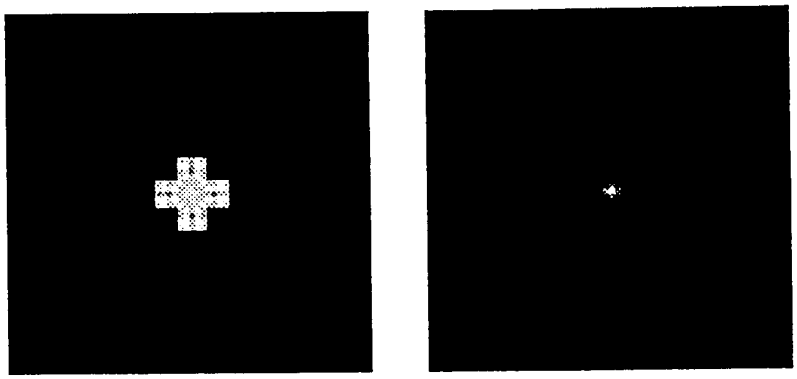

Figure 14 Semi-blind deconvolution (a) The object (b) The PSF.

The evaluated parameters for the PSF are $A_1 = 0.0508, C_1 = 1.05, C_2 = 5.07$ with 1.7% error in the evaluation of the PSF. In the case of noisy images the results in terms of fitting the correct PSF were just as good. Photon noise of about 4.0% was added to image in figure 12b. This image along with a Richardson Lucy deconvolution are shown in figure 15. 1000 iterations were used in this reconstruction.

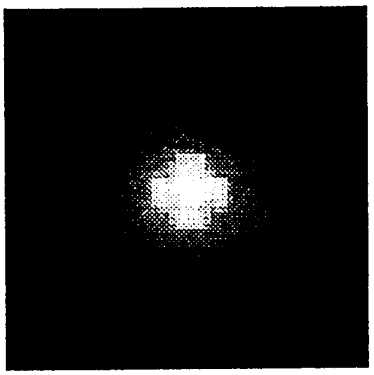

Figure 15a The image with 4.0% noise

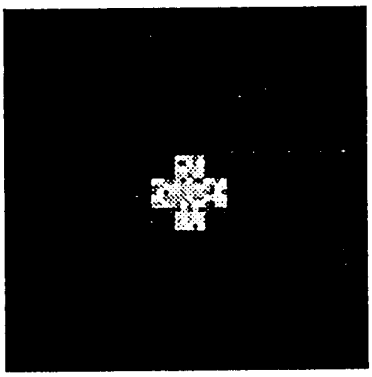

Figure 15b The Richardson Lucy deconvolution of the above image at a 4.0% noise level with 1000 iterations.

In figure 16 the result of 15 iterations of the semi-blind deconvolution method are shown. The values for the fitting parameters were $A_1 = 0.0511, C_1 = 1.056, C_2 = 5.072$ with an overall fitting error on the PSF of 1.7%.

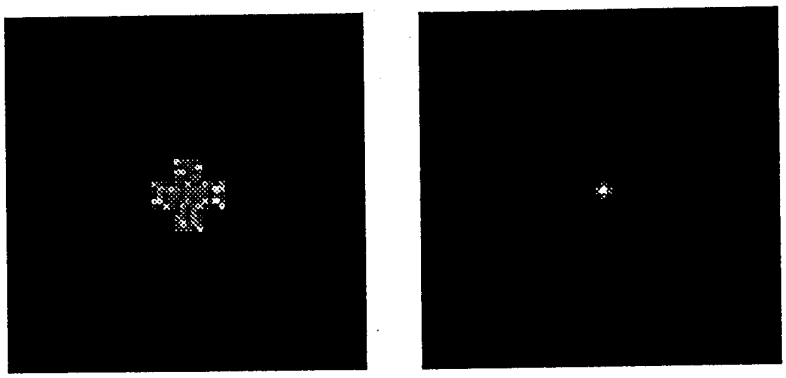

Figure 16 Semi-blind deconvolution (a) The object (b) The PSF.

In both of the above cases the semi-blind deconvolution algorithm showed definite signs of convergence. A blind deconvolution algorithm was run on the noiseless image and this did not converge to the correct result, but it did pass with 2.3% error of the correct PSF. The semi-blind algorithm was also run upon images containing 7.0% and 10% noise. Again these tests converged but to the wrong values for the fitting parameters, but it could be seen that at about 5 iterations the fitting parameters were correct. The convergence properties are shown in more detail in the next series of tests.

A second PSF was chosen and an image created. In this case the fitting parameters were slightly different $A_2 = 0.1, C_1 = 1.0, C_5 = 5.0$. This made the image rather more blurred.

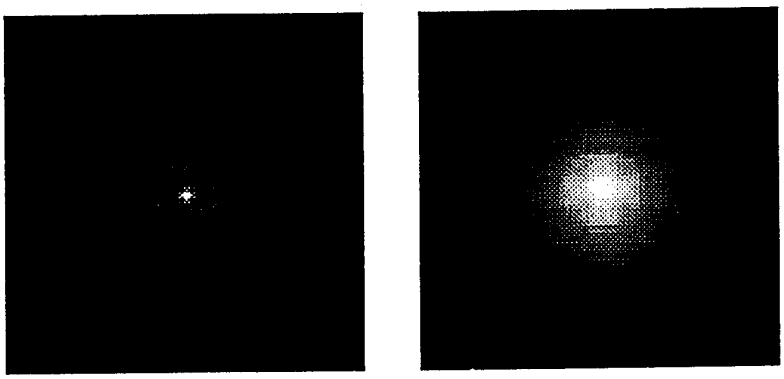

Figure 17 (a) PSF (b) Convolution with 1.0% noise.

In this case convergence was found for the noiseless case and the 1.0% noise image. The starting values entered to the program were $A_2 = 0.5, C_1 = 3.0, C_2 = 7.0$ giving a 74.0% error in the PSF. It can be seen in figures 20 and 21 that at this noise level the algorithm is converging upon the correct values. To obtain these error graphs the true PSF must be known which is slightly false since the true PSF will not be known in a real situation, but it does show the convergent properties of the algorithm. This does not occur in cases such as the Ayers-Dainty, blind Weiner and blind Richardson Lucy algorithms, see figures 3a and 3b for example. In the case of the blind Richardson Lucy algorithm the image in figure 17b was used to compare with the results of the semi-blind algorithm. It was found that the algorithm didn't converge to the correct values for the fitting parameters, and in fact the algorithm eventually diverged.

The final values for the fitting parameters of the semi-blind algorithm were $A_2 = 0.102, C_1 = 1.06, C_2 = 5.03$ with an overall error in the PSF evaluation of 1.09%. The results for the 1.0% noise image can be seen in figure 19. Figure 18 shows the reconstruction using Richardson Lucy with the real PSF, the results can be seen to compare well with those of the semi-blind deconvolution in figure 19.

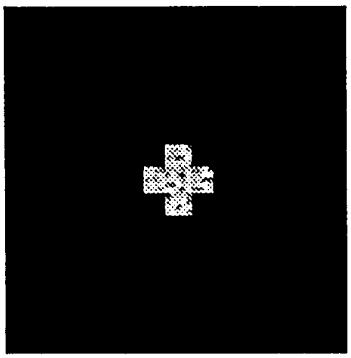

Figure 18 The Richardson Lucy deconvolution of the above image at a 1.0% noise level, with the above PSF. 1000 iterations were used.

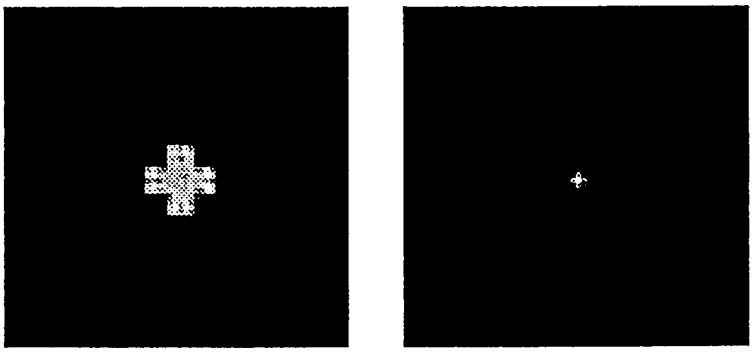

Figure 19 Semi-blind deconvolution with 1.0% noise (a) The object (b) The PSF.

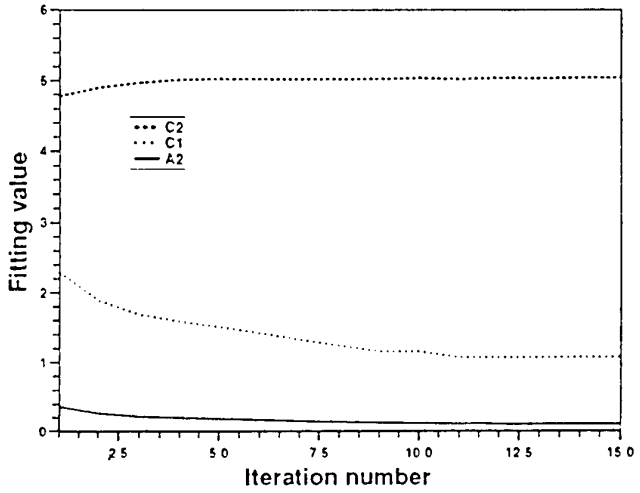

Figure 20. Variation of the fitting parameters with iteration number for 1.0% noise.

At 2.0%, 3.0% and 4.0% noise levels similar results were obtained and convergence seen at the correct values of the fitting variables. The results of the 4.0% noise image are shown in figure 23. Figure 22 shows the Richardson and Lucy deconvolution after 1000 iterations.

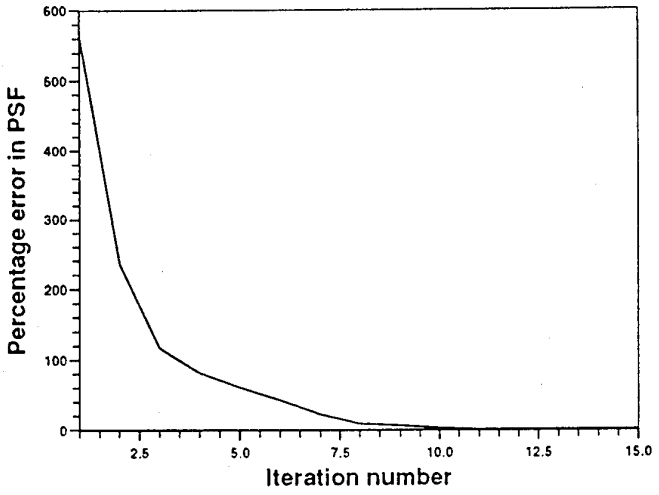

Figure 21. The error in the PSF with iteration number for 1.0% noise.

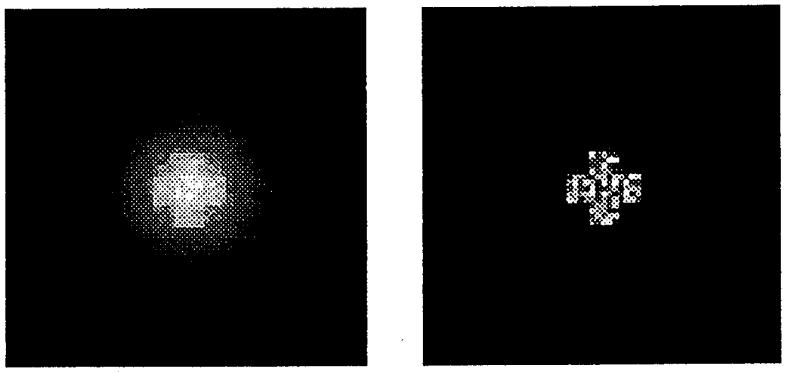

Figure 22 The Richardson Lucy deconvolution (a) The image with 4.0% noise (b) The reconstruction with 1000 iterations.

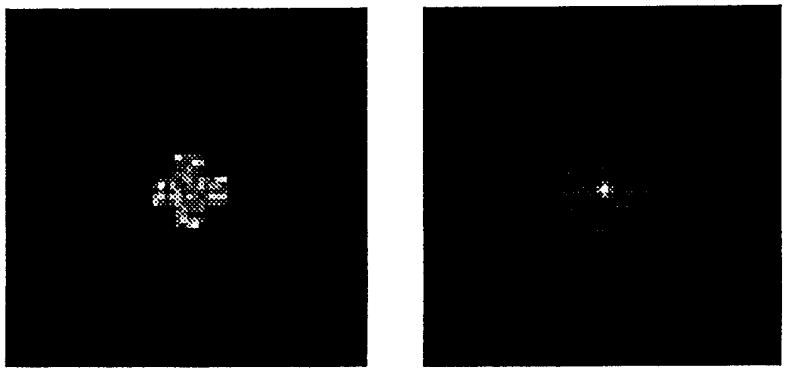

Figure 23 Semi-blind deconvolution with 4.0% noise (a) The object (b) The PSF.

Again the results compare quiet well. Figure 24 shows the variation in the fitting parameters and figure 25 the percentage error in the PSF with iteration number. Again convergence is seen. When the same image with 6.0% noise was tried, the results were not so good. Figure 26 shows the variation of fitting parameter and figure 27 the percentage error in the PSF and it can be seen that convergence is reached after 8 iterations and then the algorithm starts to diverge. It would therefore appear that the algorithm has a certain noise tolerance.

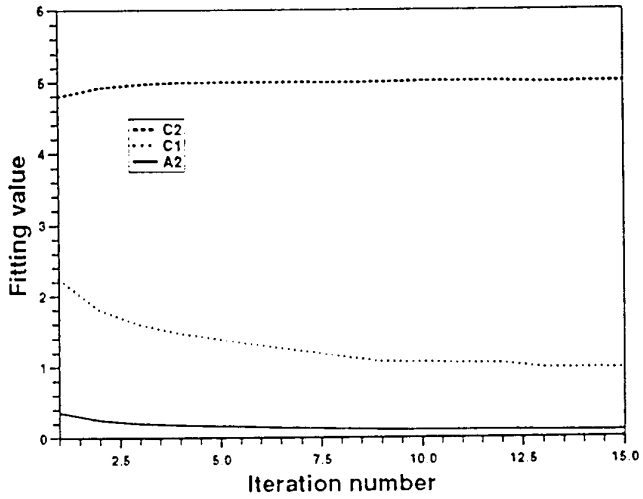

Figure 24. The variation of the fitting parameters with iteration number for 4.0% noise.

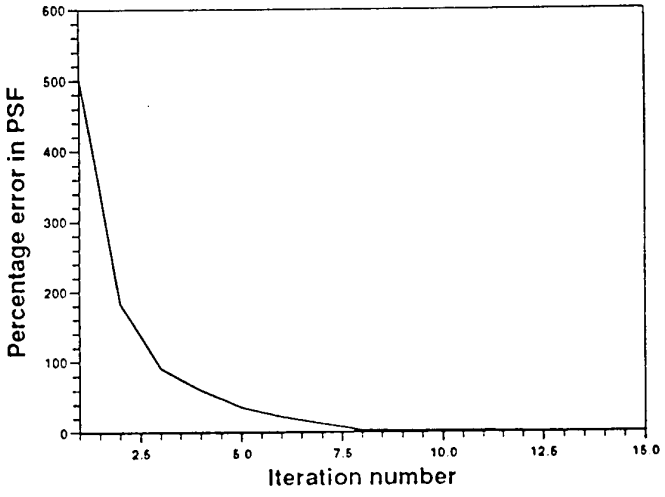

Figure 25. The error in the PSF with iteration number for 4.0% noise.

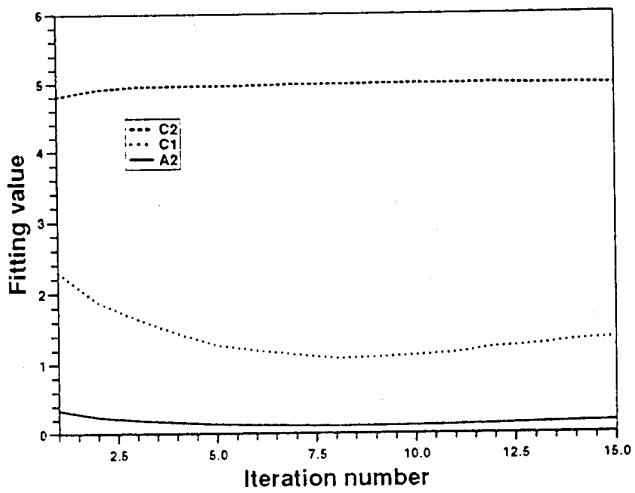

Figure 26. The variation of the fitting parameters with iteration number for 6.0% noise.

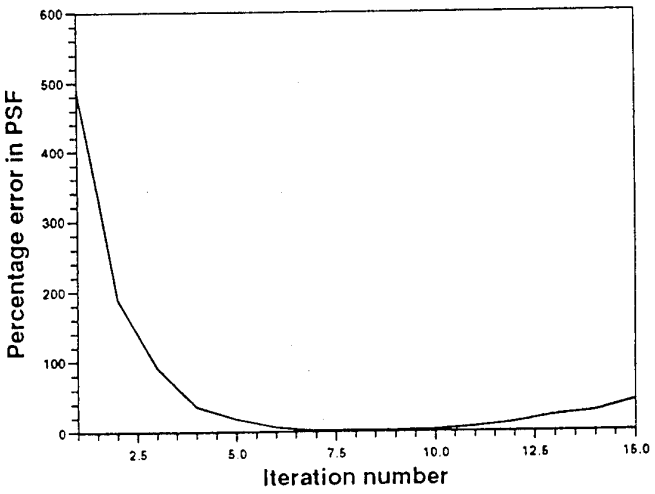

Figure 27. The error in the PSF with iteration number for 6.0% noise.

3.3 Conclusions

In many real situations it may be the case that some knowledge of the PSF can be obtained. Therefore functional forms for the PSFs were chosen with a number of unknown variables. It was found that accurate deconvolutions could be made, very near the quality of a deconvolution with full knowledge of the PSF. It appears that the extra *a priori* knowledge that the semi-blind algorithm uses stablises the

algorithm and gives it some convergent properties. It is hoped that this work can be extended to real images with PSFs containing unknown amounts of aberration where the algorithm will evaluate both the aberration coefficients and the object.

4 Image reconstruction using a known aberration function

Image restoration has been a subject intensively investigated over many years and with the increased power of computers available today remains a topic of much interest. The most recent and well publicised example of this has been the restoration of images from the Hubble space telescope (HST), before the corrective optics were added. In the case of the HST and many other imaging problems the Point Spread Function (PSF) is known. To obtain high-resolution images then requires the solution of the linear integral equation that relates the object to the image. This integral equation is known as a first-kind Fredholm equation and is a classical example of an ill-posed problem, namely a problem whose solution is affected by numerical instability and therefore is strongly noise dependant [12]. Approximate and stable solutions can be obtained using suitable techniques.

In the case of low-aperture systems an isoplanatic approximation can be made and the Fredholm equation becomes a convolution equation which is far simpler to solve. Many algorithms exist to solve this problem, there are the direct linear methods such as Tikhonov regularisation, Landweber and singular value decomposition (SVD). Among the non-linear iterative techniques are the Landweber iteration with imposed positivity, conjugate gradients and the Richardson and Lucy method [4,5]. All of the above methods except SVD generally employ the Fast Fourier Transform (FFT) for efficient computation. This allows restoration of large images because of the $nlog(n)$ speed scaling of the FFT.

In the case of real data no simple quantitative measure can be made of algorithm performance. Therefore simulated HST images were used to gain an accurate comparison of the algorithms. This work was published at a Hubble space telescope workshop in November 1993 [13]. A resume of this work is given here.

A number of methods were used to compare and contrast their performance. The methods considered were the following:-

1. Tikhonov regularisation
2. Landweber iteration
3. Landweber iteration with imposed positivity
4. conjugate gradients
5. conjugate gradients with imposed positivity
6. Richardson and Lucy

All of these methods contain a free parameter which is the so called regularisation parameter. In the first method this is essentially a parameter that reduces higher frequencies in the solution, and in the other methods it is the number of iterations. In the case of simulated images the free parameter can be chosen as the value that gives

the minimum distance in terms of euclidean norms between the approximate solution and the true solution. This then gives the best solution. In the case of real data this obviously cannot be done, so one has to choose some empirical criterion which depends upon the problem been investigated. For the simulated data used here the minimum in distance between the euclidean norm of the true and approximate solutions will be used to give the optimum regularisation parameter.

The approximate solution to the problem $\mathbf{g} = \mathbf{A}\mathbf{f} + \eta$ is given by:-

$$\mathbf{f}_\mu = \left(\mathbf{A}^\dagger\mathbf{A} + \mu\mathbf{I}\right)^{-1}\mathbf{A}^\dagger\mathbf{g} \tag{23}$$

where μ is the regularisation parameter. In case 1 Fourier transforming leaves:-

$$F_\mu(\omega) = \frac{H^*(\omega)}{|H(\omega)|^2 + \mu}G(\omega) \tag{24}$$

where $F_\mu(\omega)$ and $G(\omega)$ are the Fourier transforms of f_μ and g. $H(\omega)$ is the Fourier transform of the PSF. In case 2 the iteration scheme is given by:-

$$\mathbf{f}_0 = 0; \quad \mathbf{f}_{n+1} = \mathbf{f}_n - \tau\mathbf{r}_n \tag{25}$$

where $0 < \tau < 2||\mathbf{A}||^{-2}$ is the stationary relaxation parameter and

$$\mathbf{r}_n = \mathbf{A}^\dagger\mathbf{A}\mathbf{f}_n - \mathbf{A}^\dagger\mathbf{g} \tag{26}$$

This iterative method is equivalent to filtering since the result of n iterations can be written explicitly in Fourier space as:-

$$F_\mu(\omega) = \left[1 - \left(1 - \tau|H(\omega)|^2\right)^n\right]\frac{G(\omega)}{H(\omega)} \tag{27}$$

In method 3 this cannot be used since the imposition of positivity can only be carried out in real space, hence this algorithm requires the use of two FFTs per iteration. The relaxation parameter τ for both methods can be set as follows:-

$$\tau = \frac{1}{||\mathbf{A}||^2} = \frac{1}{|H(\omega)|^2_{max}} \tag{28}$$

where $|H(\omega)|_{max} = max_\omega|H|$. Finally the conjugate gradients iteration scheme is

$$\mathbf{f}_0 = 0; \quad \mathbf{f}_{n+1} = \mathbf{f}_n - \tau_n\mathbf{p}_n \tag{29}$$

where

$$\mathbf{p}_n = \mathbf{r}_n - \sigma_{n-1}\mathbf{p}_{n-1} \tag{30}$$

with $p_0 = r_0 = -\mathbf{A}\mathbf{g}$, $\sigma_{n-1} = ||\mathbf{r}_n||^2/||\mathbf{r}_{n-1}||^2$ and the non-stationary relaxation parameter $\tau_n = (\mathbf{r}_n, \mathbf{p}_n)/||\mathbf{A}\mathbf{p}_n||^2$. This iteration scheme can easily be written in Fourier space. The last method Richardson and Lucy was described earlier.

In the numerical experiments two test problems were considered. One of the objects was a simulated elliptical galaxy and the other was a star cluster. The simulated blurred images were obtained by convolving the object f with a calculated PSF and adding Poissonian and readout noise. The discrepancy between the reconstructed solution f^{rec} and the true solution f may be measured by the RMS norm ϵ of their difference divided by the norm of f.

$$\epsilon = \sqrt{\frac{\sum_{ij}|f^{rec}_{ij} - f_{ij}|^2}{\sum_{ij}|f_{ij}|^2}} \tag{31}$$

Algorithm	iteration number	RMS	CPU time
Richardson Lucy	1006	0.0606	21 min 18 sec
Landweber with pos.	1038	0.0484	12 min 58 sec
Landweber	direct	0.1020	2 sec
Conj. grad.	110	0.1355	2 min 5 sec
Conj. grad. with pos.	100	0.1027	1 min 52 sec
Tikhonov	direct	0.1115	1 sec

Table 1: Algorithm comparison - Star cluster image

For the direct methods the regularisation parameter is adjusted to minimize ϵ and the iterative methods are run until a minimum in ϵ is found.

The best performance for the restoration of the star cluster was provided by the Richardson Lucy and the Landweber with positivity methods. They gave accuracies of 6% and 5% respectively. The full results are shown in table 1.

These results would appear mathematically to be excellent but practically the results are far from satisfactory as many false stars appear when examining in detail. This is partially due to the fact that the solution itself is represented by discrete points, whereas the image and reconstructed solution are blurred representations thereof. In fact the choice of such solutions are particularly demanding for the restoration routines since they are delta-function like objects with sharp cut-offs. As a matter of fact the Landweber with positivity seems to perform better, this is highlighted by table 1 where it is shown that this method requires far less computational effort than the Richardson Lucy method. The other methods seem to be fast but this is at the expense of accuracy. Some example restorations are shown in figure 28 for the Richardson Lucy and Landweber with positivity methods.

In the case of the elliptical galaxy a similar set of results were obtained but this time the Richardson Lucy method seemed to out perform the Landweber with positivity method.

The mathematical problem arising from HST image restoration provides an example of inverse problems which can be fruitfully treated by regularisation techniques. Among these methods Landweber with positivity seems to provide the best compromise between accuracy and computational effort. On the other hand it is not evident from the numerical experiments performed here which is the best choice, a larger set of test problems has to be taken before making firm conclusions.

The HST was our main source of real data. One such real image was the supernova sn1987a, algorithms such as Tikhonov regularisation, Richardson Lucy etc were applied to this image. It was found that Tiknonov regularisation gave some very poor reconstructions, whereas the Richardson and Lucy method was quite impressive. In figure 29a the supernova image is shown on a log scale and the Richardson Lucy reconstruction is shown in figure 29b.

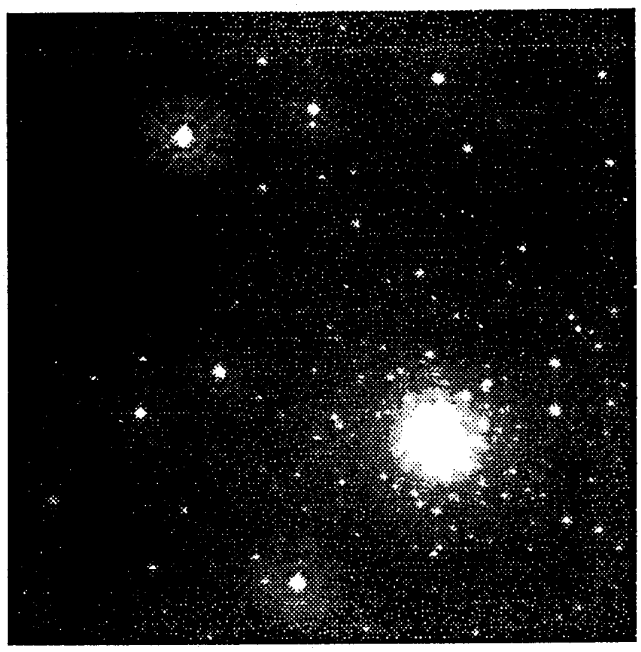

Figure 28a. The simulated star cluster image.

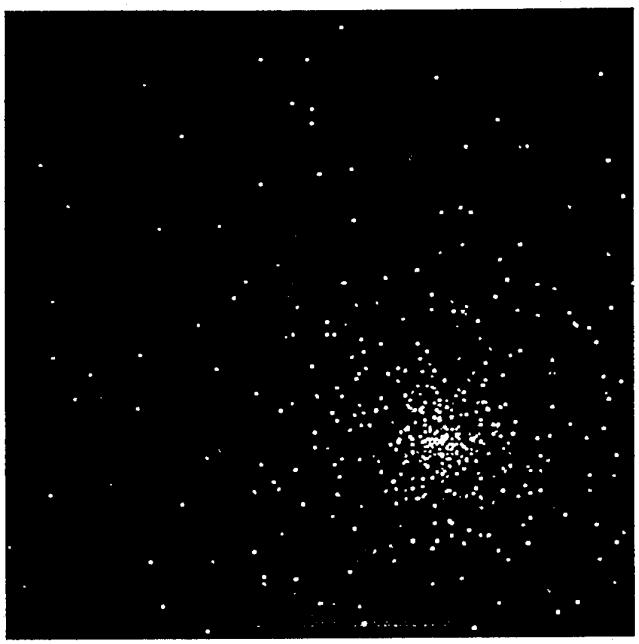

Figure 28b. The true object.

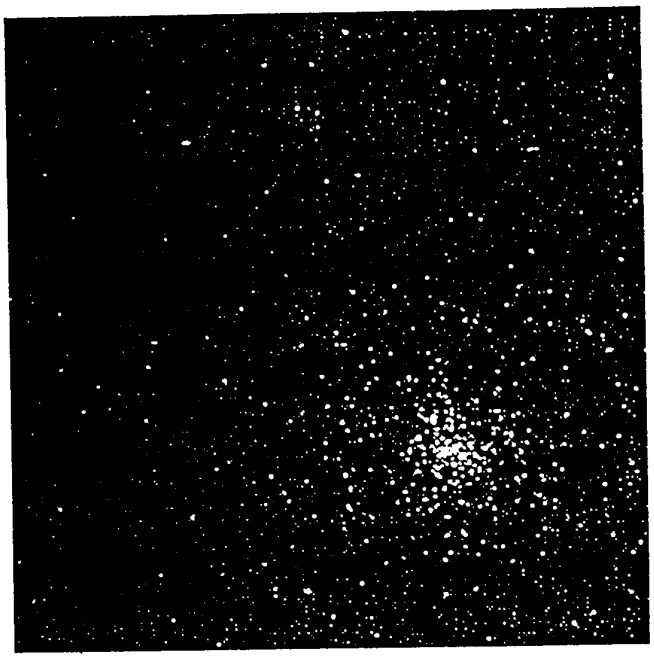

Figure 28c. The Richardson Lucy reconstruction.

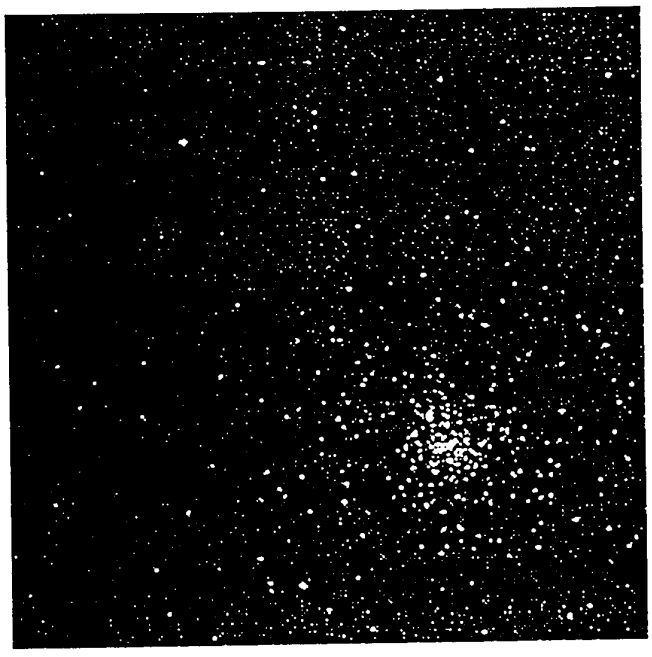

Figure 28d. The Landweber with positivity reconstruction.

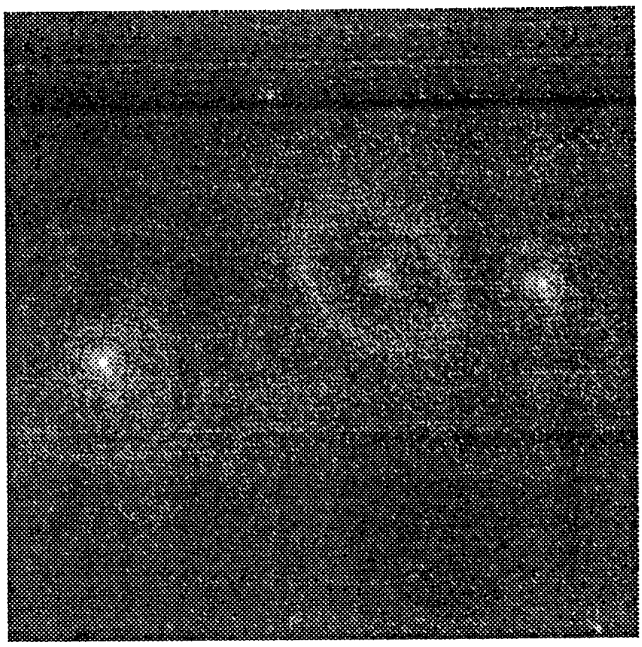

Figure 29a. The HST image of the sn1987a supernova. The intensity is scaled logarithmically.

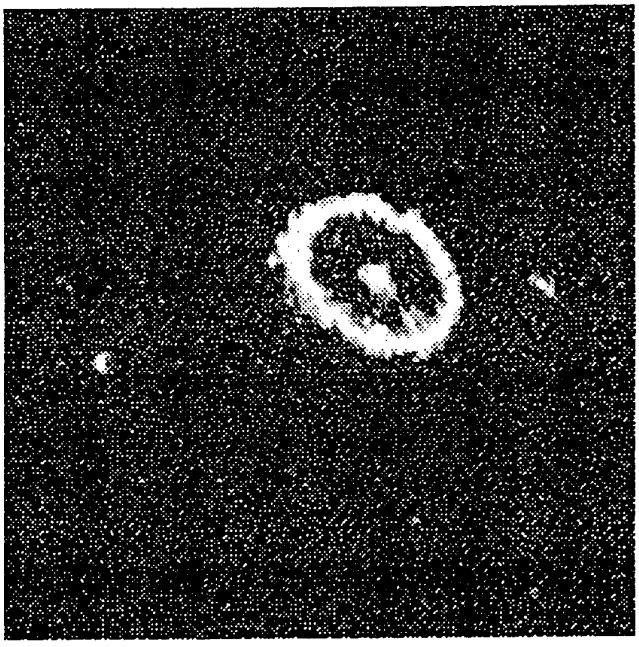

Figure 29b. The Richardson Lucy reconstruction of the sn1987a supernova. The intensity is scaled logarithmically.

5 Image reconstruction using scanning methods

A method of image reconstruction that does not rely upon the fast Fourier transform is SVD. To perform an SVD on an $n \times n$ matrix requires the order of n^3 operations, and since images require the inversion of an operator of size $n^2 \times n^2$ SVD scales as n^6. It is therefore readily apparent that the use of SVD upon large images is completely out of the question not only because of the storage requirements of an $n^2 \times n^2$ matrix but the also the extremely large times required to perform the SVD. On the other hand once the singular system of the optical arrangement has been calculated and stored, efficient high-resolution-imaging can be obtained for that system for any object. Also the SVD of the imaging system is preferable since it produces the most natural mapping from object to image space, and hence allows a suitable method to reconstruct images contaminated with noise. This is achieved with the use of a regularisation parameter or by cutting out the singular values which are below the signal to noise ratio. As a result of these points we feel that SVD methods are one of the better ways for of restoring images. Therefore a method was required that allowed the use of SVD and was computationally efficient.

5.1 Introduction

A technique was devised that scanned the image and reconstructed in parts. This relied upon the local nature of the PSF, i.e. the PSF is much smaller than the image. In most cases this is true.

We show that this technique is vastly superior to SVD in terms of the number of operations required. Also we show how the blocking effects that would normally be expected from the reconstruction of an image by parts are removed by the use of our scanning method. Reconstructions are then performed upon large complex images. Finally reconstructions are performed upon images formed with a spatially variant PSF.

5.2 Singular value decomposition in diffraction limited imaging

The linear imaging equation that we wish to solve to restore an image is the first kind linear Fredholm integral equation which can be written as,

$$g(\underline{x}) = (Hf)(\underline{x}) = \int h(\underline{x}, \underline{x}')f(\underline{x}')d\underline{x}' \tag{32}$$

where the vectors $\underline{x}$ and $\underline{x}'$ are two dimensional vectors with components (x_1, x_2) and (x_1', x_2') respectively in the data and object spaces. To simplify this equation an approximation often made is the isoplanatic approximation, which leaves equation 32 as a convolution.

$$g(\underline{x}) = (Hf)(\underline{x}) = \int h(\underline{x} - \underline{x}')f(\underline{x}')d\underline{x}' \tag{33}$$

The imaging equation can also be formulated in the discrete case as a vector-matrix problem.

$$\mathbf{g} = \mathbf{H}.\mathbf{f} \tag{34}$$

The solution of the imaging problem is the inversion of the integral operator in 32 and 33 or the matrix operator in 34. One method of approaching this problem is an eigenvalue or singular value decomposition. Here we will give a brief resume of some points relevant to image reconstruction via SVD.

If an operator A is compact and self adjoint then it maps as $\mathbf{A} : X \rightarrow X$ and a set of eigenvectors $\{u_k\}$ form an orthonormal basis in the closure of the range of A i.e $\bar{R}(\mathbf{A})$. Then for a vector in $R(\mathbf{A})$,

$$\mathbf{Af} = \sum_{k=0}^{R-1} \lambda_k \left(\mathbf{f}, u_k\right)_X u_k \tag{35}$$

where $(\cdot,\cdot)_X$ is the inner product on space X and λ_k are the eigenvalues of A. If the operators

$$\mathbf{A} = \mathbf{H}^\dagger\mathbf{H} : X \rightarrow X$$

$$\mathbf{A}^\dagger = \mathbf{H}\mathbf{H}^\dagger : Y \rightarrow Y$$

have common non-zero eigenvalues σ_k^2 and sets of eigenvectors $\{u_k\}$ and $\{v_k\}$ respectively then

$$\mathbf{H}^\dagger\mathbf{H}u_k = \sigma_k^2 u_k \tag{36}$$

$$\mathbf{H}\mathbf{H}^\dagger v_k = \sigma_k^2 v_k \tag{37}$$

where $k = 0, 1, ..., R-1$. Therefore we can always choose eigenvectors u_k and v_k such that

$$\mathbf{H}u_k = \sigma_k v_k \tag{38}$$

$$\mathbf{H}^\dagger v_k = \sigma_k u_k \tag{39}$$

Hence we have

$$\mathbf{Hf} = \sum_{k=0}^{R-1} \sigma_k \left(\mathbf{f}, u_k\right)_X v_k \tag{40}$$

$$\mathbf{H}^\dagger\mathbf{g} = \sum_{k=0}^{R-1} \sigma_k \left(\mathbf{g}, v_k\right)_Y u_k \tag{41}$$

The system $\{\sigma_k; u_k, v_k\}$ is called the singular system. The singularvectors $\{u_k\}$ span the object space and the singularvectors $\{v_k\}$ span the image space and the mapping from one to the other is controlled through the singular values σ_k. A solution still requires the inversion of the operator H. An approximate solution can be found as the unique least squares solution of minimal norm (Moore - Penrose solution) i.e,

$$\mathbf{f}^+ = \sum_{k=0}^{R-1} \frac{1}{\sigma_k} \left(\mathbf{g}, v_k\right)_Y u_k \tag{42}$$

The propagation of relative errors from data to solution is controlled by the condition number. If $\delta\mathbf{g}$ is a small variation of g the corresponding variation of f is then,

$$\frac{||\delta\mathbf{f}||_X}{||\mathbf{f}||_X} \leq cond(\mathbf{A}) \frac{||\delta\mathbf{g}||_Y}{||\mathbf{g}||_Y} \tag{43}$$

where $cond(\mathbf{A}) = \sigma_0/\sigma_{R-1}$. If $cond(\mathbf{A})$ is large the problem is said to be ill-conditioned and small variations of the data produce a completely different solution i.e. the solution is unstable to noise.

In order to find an estimate of the unknown object the effect of noise must be taken into account. Hence the true imaging equation is

$$\mathbf{g} = \mathbf{H}\mathbf{f} + \eta \tag{44}$$

where $\eta \in Y$ is the noise vector. A signal to noise ratio can then be defined as

$$\alpha = \frac{||\eta||_Y}{||\mathbf{f}||_X} \tag{45}$$

This requires that the smallest singular value of $\mathbf{H}$, σ_{R-1} be greater than α. If this condition is not satisfied then only those singular values that do satisfy this condition can be used in the reconstruction, i.e. $\sigma_K > \alpha$ and the approximate solution is given by

$$\tilde{\mathbf{f}} = \sum_{k=0}^{K-1} \frac{1}{\sigma_k} (\mathbf{g}, v_k)_Y \cdot u_k \tag{46}$$

In fact this is a linear filter to the Moore-Penrose solution

$$\tilde{\mathbf{f}} = \sum_{k=0}^{R-1} W_k u_k \tag{47}$$

where the filter contains a step function that is zero when $k > K$. Other filters can be used, such as

$$W_k = \frac{\sigma_k}{\sigma_k^2 + \epsilon\gamma_k^2} (\mathbf{g}, v_k)_Y \tag{48}$$

where ϵ is recognised as a regularisation parameter, and the γ_k are eigenvalues of a constraint operator. These are the basics of solutions via SVD. In this solution no assumption has been made about the operator $\mathbf{H}$ except that it is positive definite. In the case of a spatially invariant blur this operator has what is known as a *Block Toeplitz* structure. This can be further approximated so that the structure becomes *block circulant* i.e. the operator becomes periodic, and solutions to the imaging problem can then be found via FFTs. The solution of most imaging problems are found by making these approximations. The SVD method does not, and therefore allows the inversion of operators formed with a spatially variant PSF. As we have already mentioned conventional SVD upon reasonably sized images is at present impossible. The scanning method allows a route to the solution of this problem.

5.3 The scanning method

To overcome the speed and virtual memory requirements of SVD upon large images we have made use of the fact that in many problems the PSF is very local in nature. We also make the assumption that the PSF has a finite support within the image space. Then a far smaller portion of the singular system is required to reconstruct the image. If an appropriately sized portion of the image is taken it can be used to reconstruct the corresponding part of the object via conventional SVD.

$$\mathbf{g}_i = \mathbf{H}_i\mathbf{f}_i + \eta_i \tag{49}$$

In this equation the image vector $\mathbf{g}_i$ corresponds to a small portion of the full image and $\mathbf{H}_i$, $\mathbf{f}_i$ and η_i are the corresponding operator, object portion an noise vector.

In equation 49 the operator will be far smaller e.g. 1024×1024 for a 32×32 pixel object and image region, which allows an SVD in a reasonable time. In fact the SVD on the operator for the 32×32 image region will be $O(10^8)$ times quicker than an SVD on an operator for an image size of 512×512. After the singular system is obtained the reconstruction via equation 49 is obtained in the order of n^4 operations. The reconstruction for the 512 pixel image will require of the order 512^4 operations whereas a 512 pixel image reconstructed in 32×32 pixel parts will require of the order of $32^4 \times 16^2$ operations. This gives a factor of $O(10^2)$ in speed up. Therefore there is approximately a speed up of $O(10^{10})$.

To reconstruct the image in parts as suggested above is rather crude and the reconstructed object will contain errors due to what we call blocking effects due to the overlap of the PSF in neighbouring reconstruction areas. To overcome this problem we simply reconstruct in a smaller box so that image points outside the image box have no effect. The scanning box is the portion of the image used, the reconstruction box in chosen to lie central in the scanning box. To reconstruct the whole image the scanning box is shifted so that the next reconstruction box lies next to the previous one. In this manner the blocking effects are avoided and good reconstructions can be obtained. All that is lost is an area around the edge of the image which cannot be reconstructed as information is needed from outside the image. It must also be noted that the factor of 10^{10} speed increase will be reduced by this procedure.

As an improvement on this we also introduced an averaging method which instead of reconstructing in small boxes next to one another the reconstruction boxes were allowed to overlap. An average of the reconstructions was then taken. This allowed improvements in reconstructions as numerical errors were partially removed by the averaging process.

The operator for the segmented part of the image in equation 49 still has had no further assumptions made about its form. Therefore the spatially variant PSF problem can still be tackled with the scanning technique. In the case of a spatially invariant system only a single SVD has to be performed and the singular system can then be stored and used again. In the spatially variant PSF many SVDs have to be performed which means that the method becomes computational rather slow, but it is still accurate. In fact within this smaller area of the image the PSF should have a weakly spatially variant nature. A possible solution is then to assume spatial invariance within this area and use Fourier transforms to solve which will be far more computationally efficient.

It may also be noted that equation 49 also shows that if the image has a spatially variant noise upon it, and that noise can be considered as constant across the scanning box, then treatment of this problem is quite straightforward. All that is required some knowledge of the signal to noise ratio across the image so that a regularisation procedure can be suitably varied when reconstructing each portion of the image. This was not investigated further within this project but would be interesting to follow up

5.4 Results and discussion

To show the blocking effects mentioned in the previous section a scanning SVD was performed upon the simple image of a cross convolved with a Lorentzian of radius one pixel. Figure 30 shows the results and the errors in the reconstruction are given

in table 2. In figure 30a where the reconstruction is performed with scanning and reconstruction boxes of the same size the blocking effects are obvious and give a high reconstruction error. As the size of the reconstruction box is reduced the blocking effects disappear, and a good reconstruction is obtained with a low error as shown in figure 30f.

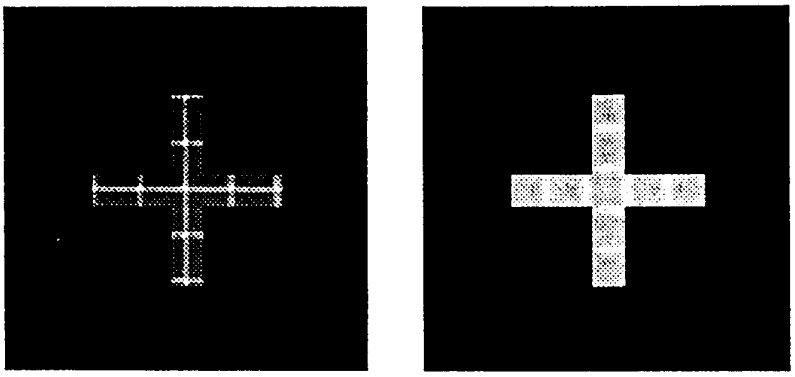

(a) Reconstruction box of size 16 × 16 pixels, 43.0% error. (b) Reconstruction box of size 14 × 14 pixels, 6.0% error.

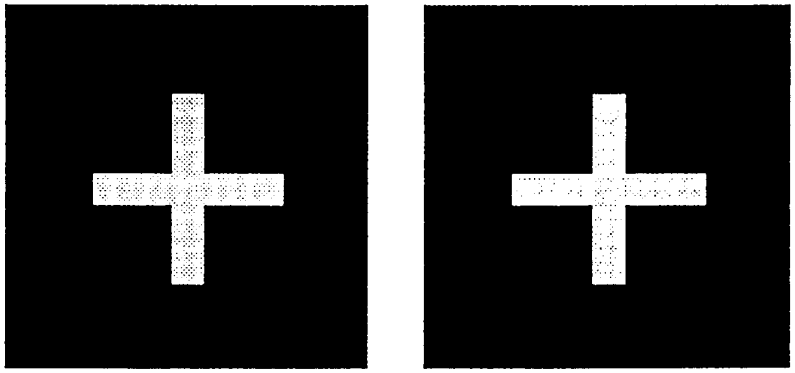

(c) Reconstruction box of size 12 × 12 pixels, 5.0% error. (d) Reconstruction box of size 10 × 10 pixels, 5.0% error.

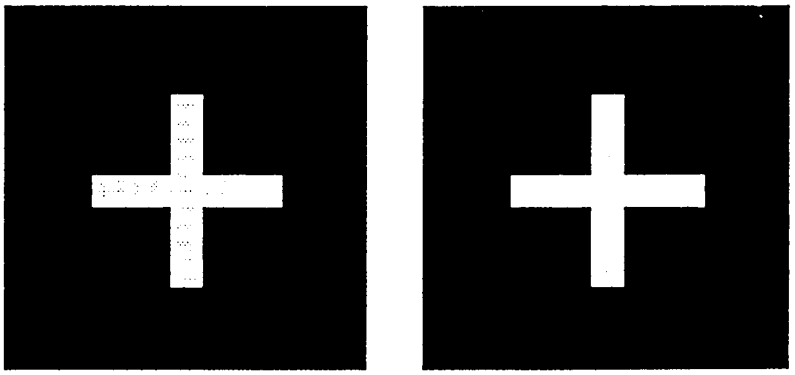

(e) Reconstruction box of size 6 × 6 pixels, 3.0% error. (f) Reconstruction box of size 2 × 2 pixels, 0.5% error.

Figure 30. The variation of reconstruction error with reconstruction box size.

Reconstruction box size	Reconstruction error
16 pixels	43.0%
14 pixels	6.0%
12 pixels	5.0%
10 pixels	5.0%
8 pixels	3.0%
6 pixels	3.0%
4 pixels	1.0%
2 pixels	0.5%
1 pixel	0.1%

Table 2: Errors in reconstruction with reconstruction box size

To show the performance upon a more complex image a 512×512 image of Lena figure 31a was obtained and convolved with a Lorentzian of radius one pixel. The image has 5.0% Gaussian white noise was added. This image can be seen in figure 31b. A reconstruction was obtained using the scanning method with a scanning box size of 32×32 pixels and a reconstruction box size of 2×2 pixels, figure 31c. In this case 157 of the available 1024 singular values were used in the reconstruction.

Figure 31a. The original Lena.

Figure 31b. Image with Lorentzian PSF of radius 1.0 pixels, condition number 138, and 5.0% Gaussian noise.

Figure 31c. A reconstruction 30.0% in error with the true image. The reconstruction was performed with a scanning box of size 32×32 pixels, and a reconstruction box of 2×2 pixels with 157 singular values.

The real advantage of this method is that it can be used to reconstruct images that are formed with a generally spatially variant blur. As mentioned earlier to do this with SVD will be very time consuming, and an approximate method which uses the same scanning idea can be performed with Fourier transforms. In this case it is then assumed that across the scanning box area that the PSF is spatially invariant. This is of course an approximation. An experiment was performed with this method upon an image blurred by a Lorentzian whose width increases with the distance from the centre of the image. The results are shown in figure 32.

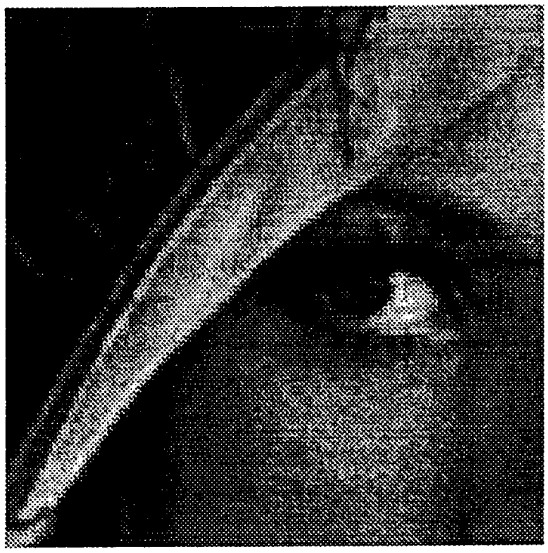

Figure 32a. The original object.

Figure 32b. An image formed with a spatially varying PSF. The PSF is Lorentzian in form with radius 1.0 pixels at the center increasing linearly to 3.0 pixels at the edge.

Figure 32c. The reconstructed image using the approximate Fourier scanning method.

The image shown is noiseless and when initial reconstructions were performed large errors occurred. This was due to the locally spatially invariant PSF approximation enforced by the use of Fourier transforms. To cope with this problem a the regularisation parameter was given a non-zero value. The departure from the spatially invariant case is then treated as noise, and controlled in the same manner. The use of SVD in reconstructing the image with spatially variant blur gives good results although it is rather computationally slow. In this case the regularisation parameter does not need altering to compensate for departures from the local spatial invariance of the PSF. An example reconstruction is shown in figure 33.

5.5 Conclusions

We have introduced a scanning method for SVD reconstruction of images. This method removes the blocking effects that would normally be associated with a reconstruction by parts. It is also vastly superior in terms of computation speed as compared with conventional SVD. The method is also applicable to the case of spatially varying blurs. The results have shown that the blocking effects are removed to a tolerable level with the scanning technique, and good reconstructions can be obtained with large complex images containing noise. To show the potential for the reconstruction of images formed with a spatially variant PSF an approximate method using Fourier transforms was shown. This introduced artifacts into the reconstruction which were controlled by use of a regularisation parameter. An example reconstruction has been shown for an SVD reconstruction which is more accurate than the Fourier method, but far slower in computational speed.

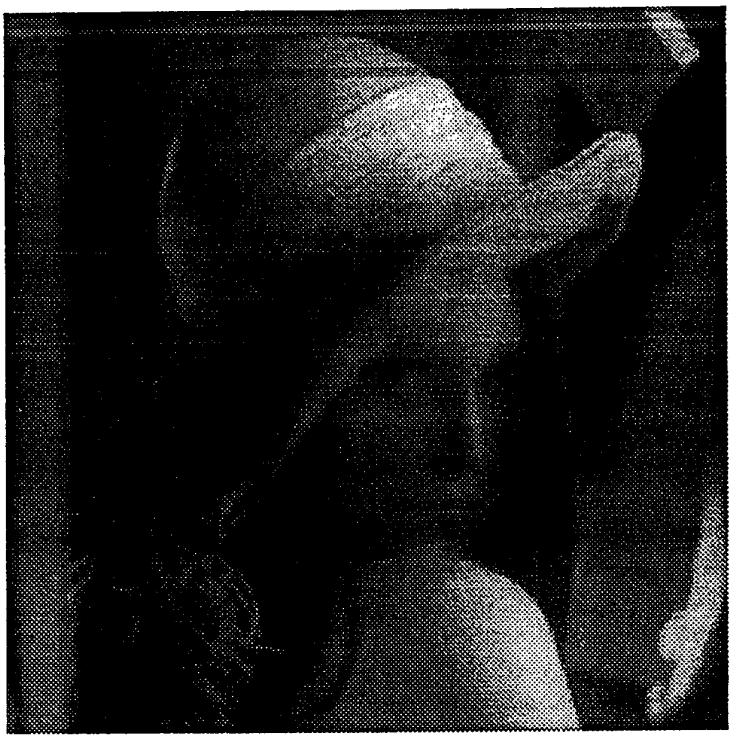

Figure 33a. The image of Lena with a spatially variant blur.

Figure 33b. The reconstruction.

6 Further work

In this contract we have investigated a number of methods for obtaining diffraction limited imaging when the optical systems are degraded, for application to such problems as for example space to space imaging. We have applied three lines of research to this problem. (i) Blind deconvolution, (ii) Image reconstruction using a known aberration function, and (iii) Exponential-filter speckle imaging. Our major effort has been upon the first two of these and we have made significant contributions to these fields.

We have investigated the performance of existing blind-deconvolution algorithms; particular issues have been robustness of algorithms to noise and the object/PSF morphology. We have also investigated a number of novel approaches to blind-deconvolution. (a) Blind deconvolution using the Richardson-Lucy (Expectation maximisation of maximum likelihood (EMML)) algorithm, and (b) semi-blind deconvolution, which makes use of further *a priori* information, i.e. having a known form for the PSF but unknown parameters describing it [10].

In the blind-deconvolution work some significant results have been obtained with the use of both full and semi-blind Richardson-Lucy algorithms [10]. In the blind case, good reconstructions have been obtained with as much as 15.0% photon noise in the image. In the semi-blind case a PSF was chosen with three free variables, where the functional form of the PSF was chosen to be a Gaussian plus a Gaussian times the radius squared. The free parameters were then the central Gaussian width, the ring width and the ring height. These parameters must be found by the algorithm. A non-linear least squares fitting routine was used at each step to find the PSF parameters, and it was found that the algorithm had convergent properties with as much as 4.0% noise upon the image. This is a great improvement upon previous blind-deconvolution work.

Image reconstruction with a known aberration function has been mainly performed upon HST images before the corrective optics were added. In terms of the BMD project the HST provided real data which would have similar deficiencies to any other orbiting optical system. A number of algorithms were considered i.e. Richardson-Lucy, conjugate gradients and Landweber with and without and positivity constraints, and Tikhonov regularisation [13]. The large size of the HST images made it impossible to use conventional singular value decomposition (SVD) methods. To overcome this limitation we have recently introduced a new technique which scans the image and produces reconstructions using SVD. The scanning SVD method reduces the computation time for image restoration by orders of magnitude without detriment to the quality of the image by exploiting the linear and local nature of the PSF. The technique is potentially of great importance because it can be used for both isoplanatic and non-isoplanatic imaging This will allow further improvement of the HST images even with corrective optics, and has application to a whole host of other imaging problems.

Experimental work has been done in the speckle imaging area. A photon limited imaging system with variable turbulence degradation has been built. It has been found in the past that detectors have been unable to cope with moving speckle patterns when trying to form the auto-correlation of the pattern due to 'dead time' effects. A detector with good 'dead time' characteristics was loaned to us by Rutherford Appleton labs (RAL). It was found that at suitable light levels the detector gave good auto-correlations with an acceptable level of noise for the moving speckle

pattern. It is now possible therefore to obtain real data in the laboratory to test algorithms.

To summarise in the current contract we have made a significant breakthrough with the new scanning SVD techniques. We have made important contributions to the technique of blind-deconvolution and we have made useful comparisons of performance for existing blind and non-blind deconvolution algorithms. We have also set up a satisfactory test bench for generating data.

Areas in which we envisage that this work could be continued is based upon the progress made with the SVD techniques for efficient image restoration in high-numerical-aperture systems, and to continue the work on blind deconvolution with the use of *a priori* information. Again these subjects have direct applicability to high resolution space imaging as well as for microscopy, astronomy and medical imaging.

For general high-numerical-aperture imaging our current work on scanning SVD techniques is directly applicable. In the case of isoplanatic imaging the scanning SVD technique has made possible for the first time the use of SVD on large images, and has made a large increase in the speed at which modest images can be reconstructed. Due to the scanning nature of the algorithm it can be generalized to high-numerical-aperture systems where the isoplanatic condition no longer exists.

One advantage of using SVD is that the singular system once calculated can be stored and high-resolution imaging performed for any object at speed. The scanning technique further improves upon this. In the non-isoplanatic case further improvements are still required. It is proposed that theoretical and computational investigations be made into the efficient SVD of matrices which are similar but not the same, which is the case when performing a scanning SVD upon an image formed by a non-isoplanatic system.

Other methods for the efficient reconstruction of images formed by optical systems with a spatially variant blur would also be of interest. One particular area which would be relevant to the scanning SVD techniques we have developed, is the concept of 'Displacement Rank' [14]. This allows the efficient inversion of Toeplitz matrices, which are the operators formed by a one dimensional spatially invariant blur. The Toeplitz structure can be relaxed and these methods still work, therefore a weakly space variant PSF system can also be inverted efficiently. The use of the scanning technique and this method should allow more general spatially variant systems to be tackled.

Another area of interest is the preconditioning of imaging operators for fast convergence. In the work of Plemmons [15], for example circulant preconditioners have been used upon block-Toeplitz operators [16], i.e the operator formed by a two-dimensional spatially invariant system. The preconditioning effectively clusters the singular values of the operator around unity so that algorithms such as conjugate gradients converge very rapidly. The investigation of preconditioning for the spatially variant PSF imaging system complement our work on SVD.

In the blind deconvolution area further investigations into the amount of *a priori* knowledge required for convergent algorithms would be a good area for further investigation. In all the algorithms to date except the semi-blind algorithm demonstrated in the current work no guaranteed convergent algorithms have been produced. The latter algorithm incorporated a large amount of *a priori* information in the functional form of the PSF. Research could be carried out to investigate the amount of *a priori* information required to give a convergent and reliable algorithm. The deconvolution process is reliable in the sense that the algorithms are convergent and

give results that, depending upon the amount of noise present, give a good representation of the object. If the problem is altered so that *a priori* information is available for both the object and PSF, how much information is required to give a reliable algorithm. To perform this some factorisation of probability distributions is required. Linnik has made significant contributions to this field [17,18] and it is hoped that these methods could be applied to the above problem.

Finally it may be practical to combine the fast linear scanning SVD method with the non-linear blind-deconvolution or other methods by use of the output values of the former as starting data for the latter. Advantages would be the satisfaction of constraints which can built into the non-linear methods without the large number of iterations normally necessary.

7 References

1. G.R. Ayers, M.J. Northcott, and J.C. Dainty - *'Knox-Thompson and triple correlation imaging through atmospheric turbulence'*, J. Opt. Soc. Am. A, Vol. 5, No. 7, p963, 1988.

2. M.J. Northcott, G.R. Ayers, and J.C. Dainty - *'Algorithms for image reconstruction from photon-limited data using the triple correlation*, J. Opt. Soc. Am. A, Vol. 5, No. 7, p986, 1988.

3. G.R. Ayers, and J.C. Dainty - *'Iterative blind deconvolution method and its applications'*, Optics Lett., Vol. 13, No. 7, p547, 1988.

4. W.H. Richardson - *'Bayesian - based iterative method of image restoration'*, J. Opt. Soc. Am., Vol. 62, No. 1, p55, 1972.

5. L.B. Lucy - *'An iterative technique for the rectification of observed distributions'*, Astro. J., Vol. 79, No. 6, p745, 1974.

6. J.R. Feinup - *'Phase retrieval algorithms: a comparison*, Appl. Opt., Vol. 21, No. 15, p2758-2769, 1st Aug. 1982.

7. B.L.K. Davey, R.G. Lane, and R.H.T. Bates - *'Blind deconvolution of noisy complex-valued image'*, Optics comm., Vol. 69, No.5,6, p353-356, 15th Jan. 1989.

8. L.A. Shepp, and Y. Vardi - *'Maximum likelihood reconstructions for Emission Tomography'*, IEEE Trans. Med. Imaging, Vol. MI-1, No. 2, p113-122, Oct. 1982.

9. A.P. Dempster, N.M. Laird, and D.B. Rubin - *'Maximum likelihood from incomplete data via the EM algorithm'*, J. Roy. Stat. Soc., Vol. 39, p1-38, 1977.

10. D.A. Fish, A.M. Brinicombe, J.G. Walker, and E.R. Pike - *'Blind deconvolution using the Richardson and Lucy algorithm'*, accepted J. Opt. Soc. Am. A, July 1994.

11. T.J. Holmes - *'Blind deconvolution of quantum-limited incoherent imagery: maximum likelihood approach*, J. Opt. Soc. Am. A, Vol. 9, No. 7, p1052-1061, July 1992.

12. M. Bertero, and E.R. Pike - *'Signal processing for linear instrumental systems with noise: A general theory with illustrations from optical imaging and light scattering problems'*, in Handbook of statistics 10 'Signal processing and its applications', Eds. N.K. Bose, and C.R. Rao, North Holland 1993, pp 1-46.

13. M. Bertero, F. Maggio, D.A. Fish, and E.R. Pike - *'Assessment of methods used for reconstructing HST images'*, in the Proceedings of the Restoration of HST images and spectra II, 18-19 November 1993.

14. T. Kailath, S. Kung, and M. Morf - *'Displacement Ranks of Matrices and Linear equations'*, J. Math. Ana. Appl., Vol. 68, pp395-407, 1979.

15. R.H. Chan, J.G. Nagy, and R.J. Plemmons - *FFT-Based Preconditioners for Toeplitz-Block Least Squares Problems*, private communication.

16. T.F. Chan - *'An Optimal Circulant Preconditioner for Toeplitz Systems'*, SIAM J. Sci. Stat. Comput., Vol. 9, No. 4, pp766-771, July 1988.

17. Y. V. Linnik - *'Decomposition of probability distributions'*, Oliver and Boyd, 1964.

18. E. Lukacs, and R.G. Laha - *'Applications of Characteristic Functions'*, No. 14 of Griffin's Statistical Monographs and Courses, Ed. M.G. Kendall, Charles Griffin and Company Limited, 1964.

8 Publications

1. M. Bertero, and E.R. Pike - *'Signal processing for linear instrumental systems with noise: A general theory with illustrations from optical imaging and light scattering problems'*, in Handbook of statistics 10 'Signal processing and its applications', Eds. N.K. Bose, and C.R. Rao, North Holland 1993, pp 1-46.

2. M. Bertero, F. Maggio, D.A. Fish, and E.R. Pike - *'Assessment of methods used for reconstructing HST images'*, in the Proceedings of the Restoration of HST images and spectra II, 18-19 November 1993.

3. D.A. Fish, A.M. Brinicombe, J.G. Walker, and E.R. Pike - *'Blind deconvolution using the Richardson and Lucy algorithm'*, accepted J. Opt. Soc. Am. A, July 1994.

4. D.A. Fish, J.A.S. Grochmalicki, and E.R. Pike - *'Efficient restoration of large images using a scanning singular value decomposition method'*, In preperation.